USING CONSTELLATION PHARMACOLOGY TO ASSESS MOLECULAR DETERMINANTS OF CELLULAR PHENOTYPES

by

Shrinivasan Raghuraman

A dissertation submitted to the faculty of
The University of Utah
in partial fulfillment of the requirements for the degree of

Doctor of Philosophy

Department of Biology

The University of Utah

August 2017

The University of Utah Graduate School

STATEMENT OF DISSERTATION APPROVAL

The dissertation of **Shrinivasan Raghuraman**

has been approved by the following supervisory committee members:

Baldomero Olivera	, Chair	**4/10/2017** Date Approved
Ayako Yamaguchi	, Member	**4/10/2017** Date Approved
David Krizaj	, Member	**4/10/2017** Date Approved
Michael Sanguinetti	, Member	**4/10/2017** Date Approved
Russell Teichert	, Member	**4/10/2017** Date Approved

and by **Denise Dearing** , Chair/Dean of

the Department/College/School of **Biology**

and by David B. Kieda, Dean of The Graduate School.

ABSTRACT

Different cell types have unique combinations of ion channels and receptors that define their physiological function. Combinations of ion channel and receptor isoforms may change in a cell-specific manner with disease progression. Thus, it is essential to design a general platform to investigate the descriptive properties of cell types and understand their role in health and disease. In this dissertation, I contributed to constellation pharmacology, a platform to assess phenotypic properties of individual cell types based on the combinations (constellations) of ion channels and receptors expressed in the plasma membrane.

To validate the platform, major cell types were identified in the pacemaking circuit of mice ventral respiratory column (VRC), a region that generates and maintains respiratory rhythm. The cell-specific constellations of three major cell types were characterized and the properties of putative inspiratory neurons were examined in intact brainstem slice preparations by electrophysiological recordings. This work revealed new neuromodulators of the respiratory pacemaking circuit that were validated using intact slice preparations.

To test the application of constellation pharmacology in identifying molecular changes in disease states, the molecular correlates of neuropathic pain were investigated. Concerted multivalent molecular changes were observed in the sensory neurons of rat dorsal root ganglia following chronic constriction injury and sciatic nerve ligation injury

that resulted in the appearance of aberrant neuronal phenotypes, which upregulated with the progression of pain states. This work demonstrated the strength of constellation pharmacology in monitoring neuronal phenotypes with the progression of disease states.

Constellation pharmacology requires the use of target selective pharmacological tools to uncover the combinations of ion channels and receptors in cell membrane. The ion channels and receptors exist in complex heteromeric isoforms for which selective pharmacological tools are not well explored. The applicability of this platform to screen for novel bioactive marine natural products with potential for targeting these ion channel isoforms was demonstrated by identifying novel neuroactive peptides from a new superfamily of snails, *Crassispiridae*.

Thus, in this dissertation, I establish the application of constellation pharmacology to 1) describe different cellular phenotypes based on the membrane constellations, 2) investigate changes to cellular phenotypes in pathological conditions and 3) discover bioactive marine natural products.

TABLE OF CONTENTS

LIST OF TABLES

LIST OF FIGURES

ACKNOWLEDGEMENTS

The dream of pursuing a PhD in biology was instilled in me by my mother, supported by my father and skillfully shaped by my teachers. Words are not enough to express my gratitude to them. My special thanks to Mrs. Jessy Kuruvilla and Dr. Vijayalakshmi Mahadevan for the rare gift of kindling passion for biological sciences.

I want to sincerely thank my committee members for encouraging my positive skills and pruning my weaknesses. Special thanks to Russ Teichert for patiently training me with techniques essential for this dissertation. I would also like to thank our collaborators from Ramirez Lab (Univ. of Washington) and Porreca Lab (Univ. of Arizona) for fruitful collaborative projects.

The members of the Olivera Lab nurtured me as their family member and I will forever be grateful to them. I am lucky to have a loving sister (Surya) and friends in Salt Lake City who made me dance, run, hike, cook, laugh and made me express myself in the most creative ways. Thank you for being as quirky as I am; I will always cherish these fond memories.

Finally, I would like to thank Prof. Baldomero Olivera. The only way to express my gratitude to Prof. Olivera is my promise to pass on my wonderful experiences to the future generation of students and scientists.

CHAPTER 1

INTRODUCTION

Understanding brain functions, in both normal and diseased states, requires elucidation of the cellular properties and the cellular interconnections that form a functional circuit. At the present time, the different cell types that form the circuitries in virtually all regions of the brain are incompletely understood and this creates a divide between molecular and systems neuroscience. In this dissertation, I helped develop an experimental approach to bridge this gap by identifying and characterizing different cell types that are present at any given locus of the nervous system based on the specific isoforms of ion channels and receptors expressed in the plasma membrane of each cell type. Describing cell types by their cell-specific combinations of receptors and ion channels has the potential to create a bridge between molecular and systems neuroscience and will provide insights into changes that occur during the development of disease states.

Cell types and constellation pharmacology

Conventionally, neuronal cell types have been defined based on morphology (eg: rod, cones, pyramidal, ganglion), neurotransmitter released (eg: cholinergic, dopaminergic, GABAergic), the person who discovered them (eg: Purkinje cell, Merkel cell, Retzius cell) or by combining electrical properties with anatomical location (eg: fast spiking neurons of striatum). From an evolutionary perspective, a cell type can be defined as "a set of cells in an organism that change in evolution together, partially independent of other cells, and are evolutionary more closely related to each other than to other cells" (1). These examples demonstrate the complexity of defining cell types and call for a comprehensive strategy to resolve this issue. Recent strategies focus on neuron-type-

specific gene batteries (called terminal selectors) that are uniquely expressed/regulated in differentiated neuronal types (1, 2). This strategy unifies many properties of cells such as enzymes for neurotransmitter synthesis, ion channels that regulate membrane potential, synaptic proteins, adhesion molecules and morphological properties like arborizations to define the core identity of a neuron, yet how these terminal selector genes are regulated remains unknown. Through a complementary approach, some cell types can be genetically labeled based on a cell-type-specific gene uniquely expressed in each cell type (3-5), but it is becoming increasingly evident that these target genes may be more broadly expressed than originally expected (6). In this dissertation, I use an experimental paradigm called constellation pharmacology to interrogate neuronal cell types. Constellation pharmacology is a term used to describe the approach of uncovering constellations (combinations) of ion channels and receptors found in different cell types that are revealed by the application of target selective pharmacology. This approach is based on the principle that different cell types uniquely express cell-specific constellations of ion channels and receptors that define their functional phenotypes.

Ion channels and receptor diversity

Constellation pharmacology aims at uncovering the combinations of ion channels and receptors that are unique to each cell type. The majority of ion channels and receptors exist in complex heteromeric isoforms that are difficult to identify due to lack of target selective pharmacological tools. Classic examples that demonstrate receptor complexity are voltage-gated potassium channels (7), nicotinic acetylcholine receptors and NMDA receptors (8-10). These ion channels and receptors are composed of different subunits

that can be assembled in various combinations, which increases receptor complexity and diversity. The contribution of these heteromeric ion channels in shaping the membrane properties of cells is largely unknown and requires target selective pharmacological tools for thorough investigation.

Conopeptides: pharmacological tools to study ion channels and receptor diversity

Cone snails are marine gastropods that evolved large cocktails of venom peptides and small molecules to capture prey and deter predators and competitors. The molecular targets of most conopeptides are receptors and ion channels in the nervous system of their prey and are excellent tools to study complex isoforms of ion channels and receptors. Several comprehensive reviews have been published that detail the molecular diversity and therapeutic potential of >10,000 species of venomous marine snails (10, 11). Inspired by the definition: cabals are secret societies plotting to overthrow the government, these groups of toxins were named toxin "cabals" based on the physiological end points achieved by a group of peptides when injected in prey ("lightning-strike cabal", "motor cabal" and "nirvana cabal" cause excitatory shock, flaccid paralysis and drowsiness respectively)(12). A well-studied species of cone snail, *Conus geographus,* elegantly explains this concept. Motor cabal of *Conus geographus* venom has these major components: ω–conotoxin GVIA, α-conotoxin GI and μ-conotoxin- GIIIA, GIIIB, GIIIC that are used together to paralyze fish by targeting neuromuscular circuitry of fish in the following three ways: 1) ω-conotoxin GVIA blocks presynaptic voltage-gated calcium channels (Cav2.2) and inhibits neurotransmitter release from the presynaptic terminus,

(2) α-conotoxin GI blocks the postsynaptic nicotinic acetylcholine receptors and prevents their activation by the neurotransmitters released by the presynaptic terminus and (3) μ-conotoxin- GIIIA, GIIIB, GIIIC directly inhibit action potentials at the muscle membrane by blocking voltage-gated sodium channels expressed in muscle membrane (13). These peptide cabals were also the inspiration for constellation pharamacology as "cabals" target "constellations" of ion channels and receptors to achieve a physiological end point. In addition to cone snails (*Conidae*), there are other venomous snails such as *Turridae, Terebridae, Colubraridae,* etc. that also have rich diversity of venom peptides, but the toxinology of these snails are yet to be explored.

Broad goals of this dissertation

By using the experimental paradigm called "constellation pharmacology", my goals are to 1) define major cell groups that network in a well-defined locus, 2) identify changes to cellular phenotypes in disease states and 3) discover new pharmacological tools for better characterization of ion channels and receptors.

<u>To use constellation pharmacology to identify cell-specific constellations of ion channels and receptors found in functional circuits</u>

Model system: ventral respiratory column (VRC) of neonatal mice

VRC in the brainstem of mice contains the pacemaker circuit that generates and maintains respiratory rhythm. It is hypothesized that within the VRC, there are specialized pacemaking circuits that control three phases of breathing: inspiration, post-

inspiration and active expiration, that are regulated by the pre-Bötzinger complex (pre-BötC), post inspiratory complex (PiCo) and the lateral parafacial nucleus, respectively (14). Of these, the pre-BötC is well studied and the application of substance-P to a slice containing the pre-BötC is known to elicit rhythmic network activity consistent with normal breathing pattern (15). Furthermore, when pre-BötC neurons in a slice are isolated from the network by blocking fast synaptic transmission, SP elicits bursting within inspiratory neurons. Thus, only a subset of preBötC neurons (putative inspiratory neurons) express the NK1 receptor (16). The circuitry contains many other cell types that are selectively active during expiration, gasping and this model system is chosen to identify cell-specific constellations in major cell types that are found in this circuitry that can be validated by electrophysiological recordings from these physiologically relevant cell types.

<u>To monitor changes to cellular phenotypes with the progression of disease states</u>

Model system: dorsal root ganglia (DRG) of adult rodents

The constellation of ion channels and receptors may change in a cell-specific manner in disease states and the goal of this project is to monitor concerted molecular changes that may occur in different cell types with the progression of disease. DRG is an excellent model system as it contains sensory neurons that relay information such as touch, itch, pain, etc. to higher centers in the nervous system. These neurons are pseudounipolar and send peripheral projections to innervate visceral organs, skin, muscle and bones (for sensory perception) and central projections to neurons within the spinal

cord that transmit sensory signals to the brain for central processing. It is hypothesized that DRG contains ~25 neuronal cell types that may be distinguished by their different physiological roles (mechanosensor, thermosensor, proprioceptor, pruriceptor, nociceptor, etc.), firing thresholds, myelination and electrical properties. In addition, various kinds of injury to DRG have been well-established as model systems to study neuropathic pain (17, 18). These injuries cause hypersensitivity to innocuous sensory stimuli and result in allodynia and hyperalgesia following nerve injury. The molecular mechanisms underlying neuropathic pain is unknown because neither the specific cell types, nor the critical molecular changes, are comprehensively identified. In this dissertation, I aim to identify changes to cellular and molecular phenotypes following neuropathic nerve injury to DRG by using two injury models: chronic constriction injury (CCI) and spinal nerve ligation (SNL).

To use constellation pharmacology to screen for novel bioactive compounds.

As described in section 1.3, venom peptides are excellent tools to study complex isoforms of ion channels and receptors. After decades of research, various conopeptides have been characterized (10). The goal of this project is to use constellation pharmacology as a platform to identify new toxins that are functionally related to previously characterized conopeptides. This approach will help expand the library of venom peptide tools to study the increasing diversity of ion channels and receptors. To test the application of constellation pharmacology in identifying new bioactive compounds, the peptides from a unique branch of venomous turrids, the family

Crassispiridae, were investigated. In particular, peptides from *Crassispira cerithina*, were tested on dissociated neurons from mice DRG and their activity was compared with previously characterized conopeptides to assess molecular targets. The biology of crasssipirine snails is not well known and only one peptide Cce9a has been reported previously (19). In this work, I tested the activity of two peptides, Cce9a and Cce9b, and compared it with previously characterized conotoxin κJ-PlXIVA (20).

References

1. Arendt D*, et al.* (2016) The origin and evolution of cell types. *Nat Rev Genet* 17(12):744-757.

2. Hobert O, Carrera I, & Stefanakis N (2010) The molecular and gene regulatory signature of a neuron. *Trends in Neurosciences* 33(10):435-445.

3. Abraira VE & Ginty DD (2013) The sensory neurons of touch. *Neuron* 79(4):10.1016/j.neuron.2013.1007.1051.

4. Le Pichon CE & Chesler AT (2014) The functional and anatomical dissection of somatosensory subpopulations using mouse genetics. *Frontiers in Neuroanatomy* 8:21.

5. Heintz N (2004) Gene Expression Nervous System Atlas (GENSAT). *Nat Neurosci* 7(5):483-483.

6. Curtice KJ*, et al.* (2016) Classifying neuronal subclasses of the cerebellum through constellation pharmacology. *Journal of Neurophysiology* 115(2):1031.

7. Coetzee WA*, et al.* (1999) Molecular diversity of K+ channels. *Annals of the New York Academy of Sciences* 868(1):233-255.

8. Lemoine D*, et al.* (2012) Ligand-gated ion channels: new insights into neurological disorders and ligand recognition. *Chemical Reviews* 112(12):6285-6318.

9. Hansen K, *et al.* (2014) Distinct functional and pharmacological properties of triheteromeric GluN1/GluN2A/GluN2B NMDA receptors. *Neuron* 81(5):1084-1096.

10. Teichert RW *et al.* (2015) CHAPTER 6 The molecular diversity of conoidean venom peptides and their targets: from basic research to therapeutic applications. *Venoms to Drugs: Venom as a Source for the Development of Human Therapeutics*, The Royal Society of Chemistry, pp 163-203.

11. Tiffany SH, *et al*. (2008) Conus venoms - A rich source of peptide-based therapeutics. *Current Pharmaceutical Design* 14(24):2462-2479.

12. Olivera BM & Cruz LJ (2001) Conotoxins, in retrospect. *Toxicon* 39(1):7-14.

13. Olivera BM (1997) E.E. Just Lecture, (1996) Conus venom peptides, receptor and ion channel targets, and drug design: 50 million years of neuropharmacology. *Molecular Biology of the Cell* 8(11):2101-2109.

14. Anderson TM & Ramirez J-M (2017) Respiratory rhythm generation: triple oscillator hypothesis. *F1000Research* 6:139.

15. Yamamoto Y, Onimaru H, & Homma I (1992) Effect of substance P on respiratory rhythm and pre-inspiratory neurons in the ventrolateral structure of rostral medulla oblongata: an in vitro study. *Brain Research* 599(2):272-276.

16. Gray PA, Janczewski WA, Mellen N, McCrimmon DR, & Feldman JL (2001) Normal breathing requires preBötzinger complex neurokinin-1 receptor-expressing neurons. *Nature Neuroscience* 4(9):927-930.

17. Mogil JS (2009) Animal models of pain: progress and challenges. *Nature Reviews Neuroscience* 10(4):283-294.

18. Decosterd I & Woolf CJ (2000) Spared nerve injury: an animal model of persistent peripheral neuropathic pain. *Pain* 87(2):149-158.

19. Cabang AB*, et al.* (2011) Characterization of a venom peptide from a Crassispirid gastropod. *Toxicon : official journal of the International Society on Toxinology* 58(8):672-680.

20. Imperial JS*, et al.* (2006) A novel conotoxin inhibitor of Kv1.6 channel and nAChR subtypes defines a new superfamily of conotoxins. *Biochemistry* 45(27):8331-8340.

CHAPTER 2

DEFINING MODULATORY INPUTS INTO CNS NEURONAL SUBCLASSES BY FUNCTIONAL PHARMACOLOGICAL PROFILING

Reprinted from:

Shrinivasan Raghuraman, Alfredo J. Garcia, Tatiana Anderson, Vernon Twede, Kigen Curtice, Kevin Chase, Jan Marino Ramirez, Baldomero Olivera and Russell Teichert. Defining modulatory inputs into CNS neuronal subclasses by functional pharmacological profiling. PNAS (2014). Vol 111 (17). p 6449-6454.

Associated Content:
Supporting Information of this paper contains experimental details and additional data, which is available at http://www.pnas.org/content/111/17/6449.long

Defining modulatory inputs into CNS neuronal subclasses by functional pharmacological profiling

Shrinivasan Raghuraman[a,1], Alfredo J. Garcia[b,c,1], Tatiana M. Anderson[b,c,d], Vernon D. Twede[a], Kigen J. Curtice[a], Kevin Chase[a], Jan-Marino Ramirez[b,c,d], Baldomero M. Olivera[a,2], and Russell W. Teichert[a,2]

[a]Department of Biology, University of Utah, Salt Lake City, UT 84112; [b]Center for Integrative Brain Research, Seattle Children's Research Institute, [c]Department of Neurological Surgery and Pediatrics, and [d]Neurobiology Graduate Program, The University of Washington School of Medicine, Seattle, WA 98101

Contributed by Baldomero M. Olivera, March 14, 2014 (sent for review January 13, 2014)

Previously we defined neuronal subclasses within the mouse peripheral nervous system using an experimental strategy called "constellation pharmacology." Here we demonstrate the broad applicability of constellation pharmacology by extending it to the CNS and specifically to the ventral respiratory column (VRC) of mouse brainstem, a region containing the neuronal network controlling respiratory rhythm. Analysis of dissociated cells from this locus revealed three major cell classes, each encompassing multiple subclasses. We broadly analyzed the combinations (constellations) of receptors and ion channels expressed within VRC cell classes and subclasses. These were strikingly different from the constellations of receptors and ion channels found in subclasses of peripheral neurons from mouse dorsal root ganglia. Within the VRC cell population, a subset of dissociated neurons responded to substance P, putatively corresponding to inspiratory pre-Bötzinger complex (preBötC) neurons. Using constellation pharmacology, we found that these substance P-responsive neurons also responded to histamine, and about half responded to bradykinin. Electrophysiological studies conducted in brainstem slices confirmed that preBötC neurons responsive to substance P exhibited similar responsiveness to bradykinin and histamine. The results demonstrate the predictive utility of constellation pharmacology for defining modulatory inputs into specific neuronal subclasses within central neuronal networks.

calcium imaging | NK1 receptor | glutamate | acetylcholine | conotoxin

Progress in understanding the mammalian brain has been impeded by the extraordinary complexity of cell types comprising the circuitry and the difficulty in bridging different levels of biological organization from the molecular to the cellular and systems level (1–4). Systems neuroscientists study the circuitry and high-level functions of the brain, whereas molecular neuroscientists study the molecular components. The large divide between these two branches of neuroscience clearly needs to be bridged to understand fully neuronal and behavioral functions in health and disease. To this end, we recently demonstrated an experimental approach we call "constellation pharmacology" to identify different neuronal subclasses by the combinations (constellations) of receptors and ion channels functionally expressed in each subclass (5–8). This experimental approach initially was applied to somatosensory neurons of the peripheral nervous system (PNS). In the present study, we use constellation pharmacology to identify neuronal subclasses of the CNS and to characterize these subclasses at the network level. Specifically, we have used constellation pharmacology to define the diverse cell types found in the mouse ventral respiratory column (VRC) and surrounding brainstem tissue.

The VRC contains a variety of neurons that are active during either inspiratory or expiratory phases of breathing. One key network within the VRC is the pre-Bötzinger complex (preBötC), which contains the circuitry essential for generating the respiratory rhythm (9–12). This network of inspiratory neurons is heterogeneous, encompassing neurons with unique pharmacological profiles (13–17). Moreover, the tissue immediately surrounding the preBötC also contains neuronal networks important to cardiovascular control, such as cardiac parasympathetic vagal neurons of the nucleus ambiguus and noradrenergic neurons of the A2/C2 region (18, 19). This anatomical convergence of networks responsible for respiratory and cardiovascular control creates an avenue through which different control elements may coordinate and couple (20) but also produces a cellular population that is heterogeneous in the responsiveness to neuromodulation.

Here we used constellation pharmacology to identify three major cell classes from the VRC and surrounding tissue. Each of these major cell classes encompasses additional subclasses that exhibit unique pharmacological profiles. We focused on one specific neuronal subclass that is responsive to substance P because substance P is an established modulator of inspiratory preBötC neurons (16). Constellation pharmacology suggested that substance P-responsive inspiratory neurons also would be responsive to histamine and bradykinin. This hypothesis was confirmed in the acute brainstem slice. Thus, this study demonstrates the utility of constellation pharmacology for investigating cell-specific constellations of receptors and ion channels expressed within neuronal and glial subclasses of the mouse brainstem and the broader potential for bridging molecular and systems neuroscience at the cellular level.

Results

Dissociated VRC Cell Cultures. We prepared cultures of dissociated VRC cells as described in *SI Materials and Methods*. Briefly, for each culture, we prepared a brainstem slice ~200 microns thick, at the level of the preBötC, from a mouse at postnatal day 7 or 8 (P7-8). We followed the same experimental approach and same protocols that we developed for producing rhythmically active

Significance

We functionally profiled cells from a locus of the mouse brainstem that contains the neuronal network responsible for generating breathing patterns. By uncovering cell-specific constellations (i.e., distinctive combinations of receptors and ion channels that define each cell type), we identified specific neuronal classes and subclasses within the network. We discovered neuromodulators affecting the activity of specific neuronal subclasses within the functional network. This study provides proof-of-principle that a pharmacological strategy for altering the activity of a specific type of neuron can be developed which has potential as a parallel or complementary approach to genetic strategies for functionally perturbing a specific neuronal cell type in vivo. Additionally, unlike genetic approaches, this pharmacological approach is directly applicable to nonmodel organisms.

Author contributions: J.-M.R., B.M.O., and R.W.T. designed research; S.R., A.J.G., T.M.A., V.D.T., and K.J.C. performed research; S.R., A.J.G., K.C., and R.W.T. analyzed data; and A.J.G., J.-M.R., B.M.O., and R.W.T. wrote the paper.

The authors declare no conflict of interest.

[1]S.R. and A.J.G. contributed equally to this work.

[2]To whom correspondence may be addressed. E-mail: olivera@biology.utah.edu or Russ.Teichert@utah.edu.

This article contains supporting information online at www.pnas.org/lookup/suppl/doi:10.1073/pnas.1404421111/-/DCSupplemental.

brainstem slice preparations (15, 17, 21). The region containing the preBötC and surrounding VRC was microdissected from the brainstem slice; then the cells were dissociated by enzymatic (trypsin) and mechanical methods. Cells were cultured overnight before calcium-imaging experiments were performed.

Fig. S1 shows images of dissociated VRC cell cultures of inadequate, optimal, and excessive density. In our hands, the optimal plating density was ~800 cells/mm^2 (not all cells survive). This plating density allowed us to perform calcium-imaging experiments in which we could monitor the individual responses of more than 100 cells simultaneously while avoiding an excessive number of cells that overlapped or made contact with neighboring cells. This optimal density enabled us to report the intrinsic responses of individual cells confidently in this study.

Calcium Imaging. Fig. S1 exemplifies a VRC cell culture that was used for a calcium-imaging experiment. The images in Fig. S1 *D–G* show the same field of view. Fig. S1*D* is bright-field image. A fluorescence image of the same cells loaded with Fura-2-AM dye (380-nm excitation and 510-nm emission) is shown in Fig. S1*E*. Fig. S1*F* is a pseudocolored ratiometric image of cells loaded with Fura-2-AM dye at rest. The ratio of fluorescence intensities at 510-nm emission, when excited alternately with 340-nm and 380-nm light, provides a relative measure of cytosolic calcium concentration, $[Ca^{2+}]_i$. Fig. S1*G* is a ratiometric image taken immediately after a stimulus to which a subset of the cells in the culture responded with an increase in $[Ca^{2+}]_i$.

The essence of the constellation pharmacology strategy is to probe a heterogeneous population of dissociated cells with a panel of selective pharmacological agents, among other physicochemical perturbations, and to monitor simultaneously the individual responses of more than 100 cells by calcium imaging. By monitoring the different response phenotypes, we can parse cell populations into major cell classes and minor subclasses.

Pharmacological Profiling of VRC Cells. Fig. 1 exemplifies calcium-imaging traces from selected VRC cells in response to a set of receptor agonists and to depolarization by a high concentration (e.g., 100 mM) of extracellular potassium (high $[K^+]_o$). Abbreviations and concentrations for each of the pharmacological agents and other cellular perturbations used in this study are summarized in Table 1. Three major classes of cells within these cultures could be differentiated by their distinct response profiles.

The first major cell class, class A, was defined by responsiveness to high $[K^+]_o$ and by the lack of responses to a panel of receptor agonists (Fig. 1*A* and Table 2). The second major cell class, class B, was defined by responsiveness to high $[K^+]_o$ and one or more receptor agonists tested (Fig. 1*B* and Table 2). Notably, responsiveness to glutamate was excluded as a criterion for classifying cells, because ~75% of both class A and class B cells responded to glutamate. However, only class B cells responded to the other receptor agonists (Table 2). In fact, the majority of class B cells responded to each of the receptor agonists, with the exceptions of the neuropeptides substance P and bradykinin, to which a minority of the class B cells responded (Table 2).

On average, class A cells responded to depolarization by high $[K^+]_o$ with large, transient increases in $[Ca^{2+}]_i$ (Fig. 1*A* and Table 2), indicating that they express high levels of voltage-gated calcium channels as is characteristic of neurons. On average, class B cells responded less strongly than class A cells to depolarization by high $[K^+]_o$ (Fig. 1*B* and Table 2). This difference was statistically significant (P value = 0.001, Student t test). At present it is unclear whether class B cells are all neurons or are a mixed population of neurons and glia.

The third major cell class, class C, comprises putative nonneuronal cells (glial cells and potentially other nonneuronal cells) that did not respond to depolarization by high $[K^+]_o$ or responded very weakly (i.e., a change in 340/380-nm ratio <0.1) (Fig. 1*C* and Table 2), suggesting that, unlike neurons, they do not express voltage-gated calcium channels or express these channels at very low levels. A small minority of class C cells responded to each of the receptor agonists tested (Table 2). However, when we reduced the resting $[K^+]_o$ from 3 mM to 0.2 mM, 30% of the class C cells responded with an increase in $[Ca^{2+}]_i$ (Fig. S2). Such responses (putatively mediated by $K_{ir}4.1$) have been shown to be specific to astrocytes in the VRC (22, 23). This evidence supports the hypothesis that many class C cells are glial (astrocytes and other glial cells). Furthermore, none of the class A cells responded to 0.2 mM $[K^+]_o$, thus supporting the hypothesis that class A cells are all neurons. However, 6% of the class B cells responded to 0.2 mM $[K^+]_o$, suggesting that some of the class B cells are astrocytes.

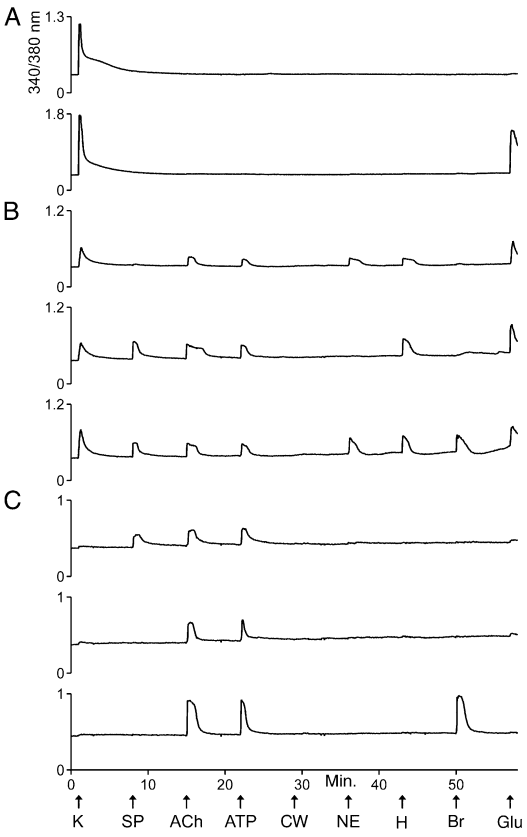

Fig. 1. Examples of calcium-imaging traces from dissociated VRC cells in culture. Each trace is the response of a single cell to the experimental protocol depicted at the bottom of the figure. In each experimental trial, the individual responses of >100 cells were monitored simultaneously. The *x*-axis and experimental protocol at the bottom of the figure apply to all traces in the figure. The units of the *x*-axis are time in minutes. The arrows identify time points when various types of stimuli were applied to the cells for 15 s. The abbreviations for these stimuli are defined in Table 1. "CW" represents a control wash, i.e., the replacement of bath solution (artificial CSF, aCSF) with identical bath solution. The *y*-axis for each trace is the ratio of fluorescence intensities obtained at 510-nm emission from the alternating excitation by 340-nm or 380-nm light. It is a measure of relative changes in $[Ca^{2+}]_i$. (*A*) Examples of traces from class A cells. Both cells responded strongly to depolarization by high $[K^+]_o$, but only one responded to glutamate with an increase in $[Ca^{2+}]_i$. (*B*) Examples of traces from class B cells. Notably, these cells responded less strongly than class A cells to high $[K^+]_o$. They typically responded to several receptor agonists, as shown. (*C*) Examples of traces from class C cells. These cells either did not respond to depolarization by high $[K^+]_o$ or responded very weakly.

Table 1. Abbreviations of compounds cited in figures and tables

Abbreviation	Compound	Working concentration
ACh	Acetylcholine	1 mM
ArIB	α-Conotoxin ArIB[V11L;V16D]	200 nM
ATP	Adenosine 5′ triphosphate	20 μM
Br	Bradykinin	10 μM
CW	Control Wash	NA
Glu	Glutamate	300 μM
H	Histamine	50 μM
K	$[K^+]_o$	100 mM
NE	Norepinephrine	20 μM
NMDA	*N*-methyl-D-aspartate and	100 μM
D-ser	D-serine	10 μM
PNU	PNU-120596	5 μM
SP	Substance P	1 μM

Cluster Analysis of VRC Cells. With the eight stimuli shown in Fig. 1, it theoretically is possible to identify 256 unique cell-response profiles, but 103 unique response profiles actually were observed. We first grouped these 103 response profiles into three broad cell classes, A, B, and C, as described above and as shown in Table 2. We then performed cluster analysis to determine whether these broad cell classes were supported by an unbiased data analysis. The cluster analysis included 1,586 cells, representing the 103 unique response profiles, which clustered robustly into three broad cell classes in all 500 bootstrap trials. These broad cell classes were consistent with our original designations of cell classes A, B, and C.

As a lower bound on the number of unique cell profiles robustly identified, we estimated the number of clusters required to explain most of the variation in cell responses. The cluster analysis summarized in Table S1 grouped cells into 36 clusters that explain 99% of the cell responses. We then sorted those 36 clusters from Table S1 into broader groups that essentially correspond to our original assignments of class A cells (the top two clusters), class B cells (the middle 24 clusters), and class C cells (the bottom 10 clusters). Notably, for each cluster shown in Table S1, the predominant response profiles (the prototype response profile) and the mean responses to depolarization by high $[K^+]_o$ (the mean K^+ response) agree with these broader cell class designations.

Comparison of VRC and DRG cells. For direct comparison with VRC cells, we conducted the profiling protocol shown in Fig. 1 with cultures of dorsal-root ganglion (DRG) cells from mice of the same age (P7-8). Table 2 shows the direct comparison between VRC and DRG cells in response to the same panel of pharmacological agents. We divided DRG cells into a combined class A/B group and a separate class C group. The distinction between class A and B cells that was obvious in the VRC was not evident in the DRG. Furthermore, in the DRG, the cell bodies of the neurons are morphologically distinct from the other cell bodies in the culture: The neuronal cell bodies are larger in diameter than the nonneuronal cell bodies and are rounder than the cell bodies of the satellite glial cells, which are relatively flat and elongated (24). Therefore, we can conclude that in DRG cultures the class A/B cells are neurons and the class C cells are various nonneuronal cells.

There are several notable points of comparison and contrast between VRC and DRG cultures from P7-8 mice (Table 2): A very high percentage of the class C cells in DRG cultures responded to ATP, in contrast to the low percentage of ATP-responsive class C cells in VRC cultures. In VRC cultures, the majority of the class B cells and a small subset of class C cells responded to norepinephrine with an increase in $[Ca^{2+}]_i$, but almost none of the DRG cells responded to norepinephrine in this way. In VRC cultures, the majority of class A and B cells responded to glutamate, in contrast to the low percentage of glutamate-responsive class A/B cells in DRG cultures. A qualitative assessment of the glutamate responses indicated that the glutamate responses in VRC cells were relatively large compared with the very small responses observed in DRG cells. Other interesting points of comparison and contrast are shown in Table 2.

Acetylcholine-Receptor Expression in VRC Cell Classes. In addition to the experimental protocols shown in Fig. 1 and Fig. S2, we investigated the expression of acetylcholine (ACh) receptors (AChRs) in VRC cells (Fig. S3). We observed that responses to ACh were blocked by atropine, suggesting that these responses were mediated primarily by muscarinic acetylcholine receptors (mAChRs) and not nicotinic acetylcholine receptors (nAChRs) (Fig. S3). When the cells were preincubated with a positive allosteric modulator of α7 nAChRs, PNU-120596 (PNU), then a different subset of cells responded to ACh. Notably, α7 nAChRs desensitize very rapidly upon application of ACh (25). Such rapid desensitization may prevent a measurable increase in $[Ca^{2+}]_i$ in the absence of PNU. To confirm that the ACh responses in the presence of PNU were mediated by α7 nAChRs, we blocked the responses with the highly subtype-selective blocker of α7 nAChRs, α-conotoxin ArIB[V11L;V16D] (Fig. S3) (26).

As shown in Fig. S3, we divided VRC cells into classes A, B, and C, on the basis of their responses to high $[K^+]_o$, ACh (before PNU application), substance P (as shown in Fig. S3), and norepinephrine. Cells were classified as class A if they responded only to high $[K^+]_o$ and as class B if they responded to high $[K^+]_o$ and to ACh (before PNU application) or substance P or

Table 2. Summary of responses from the profiling experiments depicted in Fig. 1

	Criteria for classification				% responsive cells in each cell class						
Cell class	Average response to 100 mM $[K^+]_o$ ± SD	Responsiveness to pharmacological compounds	Total cells	% of total cells	SP	ACh	ATP	NE	H	Br	Glu
Ventral respiratory column (P7-8 mouse)											
Class A	0.8 ± 0.4	Responsive to glutamate only and response to 100 mM $[K^+]_o > 0.1$	220	13	0	0	0	0	0	0	78
Class B	0.3 ± 0.2	Responsive to other receptor agonists and response to 100 mM $[K^+]_o > 0.1$	574	33	8	91	68	65	74	35	76
Class C	0.0 ± 0.0	Response to 100 mM $[K^+]_o < 0.1$	965	55	1	6	8	4	5	6	6
Dorsal root ganglia (P8 mouse)											
Class A/B	Responsive	Response to 100 mM $[K^+]_o > 0.1$	787	32	0	7	76	1	6	27	3
Class C	0	Response to 100 mM $[K^+]_o < 0.1$	1,673	68	0	7	86	0	0	5	0

The average response to 100 mM $[K^+]_o$ ± SD is a relative measure of the change in $[Ca^{2+}]_i$ elicited by 100 mM $[K^+]_o$ (i.e., change in the 340/380-nm ratio shown in figures and described in *SI Materials and Methods*). Larger numbers indicate a greater response or greater relative change in $[Ca^{2+}]_i$ elicited by high $[K^+]_o$. The VRC dataset was compiled from five independent experimental trials using cells prepared separately from four different mice. The DRG dataset was compiled from six independent experimental trials using cells prepared separately from two different mice. ACh, acetylcholine; Br, bradykinin; Glu, glutamate; H, histamine; NE, norepinephrine; SP, substance P.

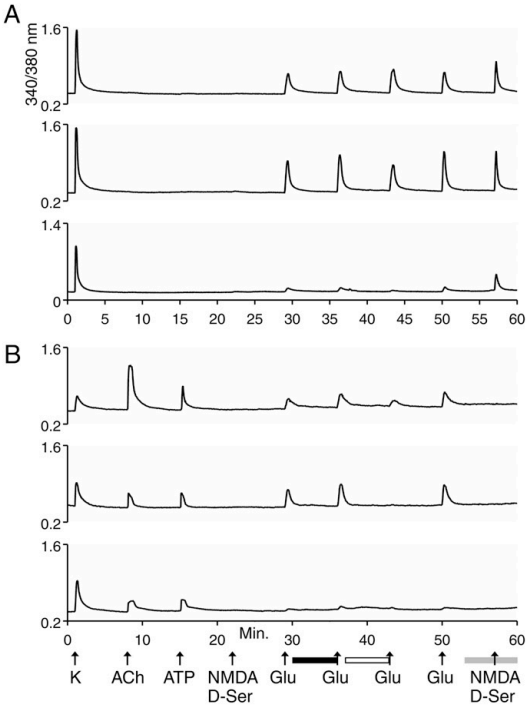

C

Cell Class	Avg Resp. to 100 mM $[K^+]_o$	% of Total Cells	% of responsive cells in each cell class: NMDA-R	Non-NMDA-R	Glu Resp. Blocked by CNQX (>5% block)	Avg %block by CNQX(S.D.)
A	1.2	7%	49%	51%	84%	60% (31%)
B	0.3	30%	6%	84%	99%	81% (24%)
C	0.0	63%	0%	1%	99%	89% (16%)

Fig. 2. Examples of calcium-imaging traces from experiments investigating glutamate receptors in dissociated VRC cells presented as in Fig. 1. (*A*) Examples of traces from class A cells. (*B*) Examples of traces from class B cells. In *A* and *B* there was no response to NMDA/D-ser in the presence of Mg^{2+} at minute 22 (because Mg^{2+} blocks NMDA receptors without a depolarizing stimulus; compare with NMDA/D-ser application at minute 57 in the absence of Mg^{2+}), indicating that the subsequent responses to 300 μM glutamate were mediated by AMPA/kainite receptors and/or metabotropic glutamate receptors. The black horizontal bar below the *x*-axis indicates the presence of 100 μM AP5 (an NMDA receptor inhibitor) in the bath. The presence of 100 μM AP5 did not block the response to the second application of 300 μM glutamate, confirming that these responses were not mediated by NMDA receptors. The open horizontal bar below the *x*-axis indicates the presence of 10 μM CNQX (an AMPA/kainite receptor inhibitor) in the bath. In general, CNQX partially blocked glutamate-elicited responses, indicating expression of a mix of AMPA/kainite receptors and metabotropic glutamate receptors. The gray horizontal bar below the *x*-axis indicates the time point when the bath solution (aCSF) was changed to Mg^{2+}-free aCSF. The application of NMDA/D-ser in the absence of Mg^{2+} demonstrated that about half of class A cells but only a small minority of class B cells expressed NMDA receptors. (*C*) Compilation of data for class A and B cells. This dataset was compiled for 2,483 cells from eight independent experimental trials, using cells prepared separately from five different mice. Notably, there are some minor discrepancies between the data compiled in *C* from the experimental protocol depicted in *A* and *B* and the data compiled in Table 2 from the experimental protocol depicted in Fig. 1; these discrepancies demonstrate a range of experimental variability.

norepinephrine. Class C cells were determined by the same criterion used in Table 2, a change in the 340/380-nm ratio <0.1 in response to high $[K^+]_o$. On average, the class A cells exhibited greater responses to high $[K^+]_o$ than class B cells, as expected and as demonstrated in Fig. S3*D*. None of the class A cells responded to ACh before the application of PNU. However, after preincubation with PNU, the majority of class A cells (66%) began to respond to ACh, indicating that they express functional α7 nAChRs (Fig. S3 *A* and *D*). In contrast to class A cells, the majority of class B cells (73%) responded to ACh before PNU application. Those responses were blocked by atropine, indicating that the majority of class B cells express functional mAChRs (Fig. S3 *B* and *D*).

Glutamate-Receptor Expression in VRC Cell Classes. For the following experiments exploring glutamate-receptor expression, cells were parsed into classes A, B, and C by the following criteria: Cells were considered class A if they responded only to high $[K^+]_o$ and as class B if they responded to high $[K^+]_o$ and either ACh (in the absence of PNU) or ATP (Fig. 2). Class C cells were determined by the criterion used in Table 2, a change in 340/380-nm ratio <0.1 in response to high $[K^+]_o$. On average, the class A cells exhibited greater responses to high $[K^+]_o$ than class B cells, as expected and as demonstrated in Fig. 2*C*. Notably, approximately half of class A cells were found to express functionally NMDA receptors [see response to NMDA/D-serine (D-ser) at minute 57 in Fig. 2 *A* and *C*] and metabotropic glutamate receptors [for the portion of glutamate-elicited response not blocked by 6-cyano-7-nitroquinoxaline-2,3-dione (CNQX) in Fig. 2*A*], with or without detectable expression of non-NMDA (AMPA or kainate) receptors (for the portion of glutamate-elicited response blocked by CNQX in Fig. 2 *A* and *C*). The majority of class B cells functionally expressed AMPA and/or kainite receptors, but only a small minority expressed NMDA receptors (Fig. 2 *B* and *C*). Class C cells did not express NMDA receptors (Fig. 2*C*).

From Dissociated Cells to Functional Networks. Histological studies within the VRC demonstrate that neurokinin-1 receptors within this brainstem region are concentrated most densely at the level of the preBötC (27–29) and that the application of substance P to the preBötC stimulates both rhythmic network activity and excitability of synaptically isolated preBötC neurons in the brainstem slice preparation (16, 27). Thus, we focused on class B cells within our dissociated cell preparations that responded to substance P. Fig. 1*B* and Table S1 demonstrate that there were two main clusters (or subclasses) of substance P-responsive (class B) cells. Although both cellular subclasses were responsive to histamine, only one was responsive to bradykinin (Table S1). Thus, we hypothesized that histamine and bradykinin may directly modulate the activity of inspiratory preBötC neurons. Patch-clamp recordings were made from inspiratory preBötC neurons in rhythmically active brainstem slice preparations. When these neurons were identified in the functional network, they were isolated from fast synaptic transmission. Fig. 3 shows that histamine and bradykinin exhibited neuromodulatory effects in inspiratory neurons that also were responsive to substance P. Histamine or bradykinin changed firing patterns and increased the firing rate of many inspiratory neurons (Fig. 3). Moreover, as is consistent with the dissociated-cell experiments, substance P-responsive inspiratory neurons within the brainstem slice exhibited a variable sensitivity to bradykinin, as illustrated in the bradykinin response alone (Fig. 3 *B* and *C*) and when comparing

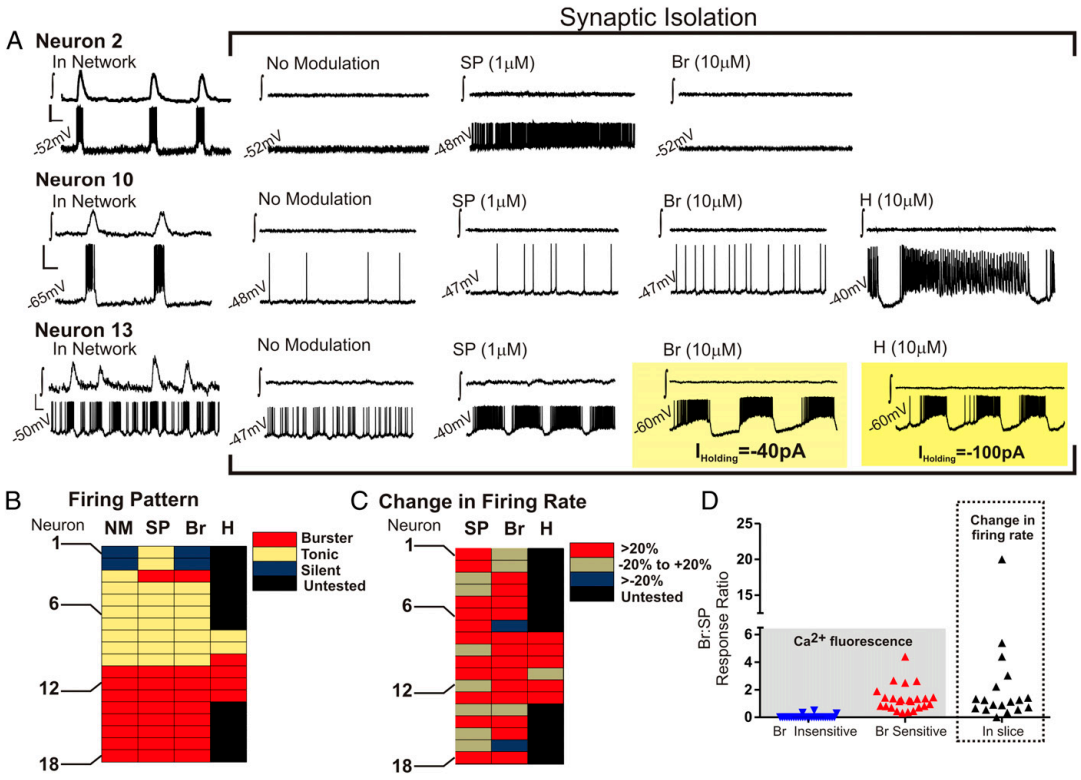

Fig. 3. The effects of substance P, bradykinin, and histamine on inspiratory neurons of the preBötC within a brainstem slice preparation. (*A*) Electrophysiology traces are shown in pairs from the preBötC population (∫, upper trace in each case) and a single inspiratory neuron of the preBötC (lower trace in each case) during synaptic isolation, without modulation, and in response to substance P (SP; 1 μM), bradykinin (Br; 10 μM), and histamine (H; 10 μM). (*Top*) Neuron 2 is silent in the absence of exogenous neuromodulation, is stimulated in the presence of substance P to exhibit a tonic firing pattern, is silent in the presence of bradykinin, and was not tested in the presence of histamine. (*Middle*) Neuron 10 is tonic in the absence of exogenous neuromodulation. Although both substance P and bradykinin stimulate a tonic firing rate, histamine changes the tonic firing pattern to a burster phenotype. (*Bottom*) Neuron 13 exhibits a burster phenotype in the absence of exogenous neuromodulation. Substance P stimulates the burster phenotype, whereas both bradykinin and histamine caused Neuron 13 to depolarize (>1.5 mV), requiring the injection of a hyperpolarizing current to prevent depolarization block. [Scale bars: 1 s (*x*-axis) and 20 mV (*y*-axis).] (*B–D*) Summaries of isolated inspiratory neurons ($n = 18$). These summaries demonstrate the diverse effects of substance P, bradykinin, and histamine on synaptically isolated inspiratory neurons. Examples of silent, tonic, and burster firing patterns are shown in *A*. (*B*) Firing pattern. (*C*) Change in firing rate. (*D*) Comparison of bradykinin responses as a ratio of substance P responses from individual substance P-sensitive dissociated cells (*Left*) and inspiratory preBötC neurons within the brainstem slice preparation (*Right*).

the individual bradykinin response with that of the respective substance P response (Fig. 3*D*).

Discussion

The results shown in Fig. 3 have two broad implications. (*i*) Constellation pharmacology can identify neuronal subclasses in dissociated cultures that maintain specific properties of neuronal subclasses within an organized network. (*ii*) Constellation pharmacology can be used to generate hypotheses that are testable, and in this case confirmed, within more intact systems. In conjunction with our prior studies of the PNS (5–8), this study suggests that constellation pharmacology may be applied productively to any locus of the CNS. Thus, our ultimate goal is to use constellation pharmacology broadly across different organisms, in different anatomical loci, and at different stages of development to characterize single cells by elucidating their cell-specific constellations of signaling proteins.

Previously, we reported a similar characterization of cells from mouse DRG (5–7), which we recently have extended to both trigeminal ganglia (TG) and DRG at different developmental stages (8). In the latter study, neurons from a genetic model organism (mouse) were compared with homologous neurons from a non-model organism (rat). In this report, we have extended constellation pharmacology to the comparison of cellular subclasses in the CNS and PNS. In contrast to the DRG and TG neurons that transduce many different sensory modalities from the periphery to the brain, the VRC comprises neuronal networks with integrated physiological functions, i.e., cardiorespiratory control. Not surprisingly, the constellations of DRG cells are strikingly different from the constellations of VRC cells (Table 2).

In this study, we initiated the classification of different VRC cell types within the mouse brainstem at the level of the preBötC. We have identified three major cell classes: A, B, and C. Class A cells, on average, were strong responders to a depolarizing stimulus. The majority also responded to glutamate but not to any of the other receptor agonists tested in Fig. 1 (see Table 2). However, after preincubation with PNU, the majority of class A cells began to respond to ACh, indicating that they express α7 nAChRs (Fig. S3). In contrast to class A cells, class B cells, on average, were relatively weaker responders to a depolarizing

stimulus, and the majority of class B cells responded to several different receptor agonists (Fig. 1, Table 2, and Table S1). Class C cells either did not respond to a depolarizing stimulus or responded very weakly, suggesting that they include glial cells and potentially other nonneuronal cells (Fig. 1 and Table 2). A subset of class C cells (30%) responded to 0.2 mM $[K^+]_o$, suggesting that many of these cells are astrocytes (Fig. S2).

Within class B, the substance P-responsive neuronal subclasses are of particular interest because of their putative roles in generating the breathing pattern within the preBötC. Although the neurokinin-1 receptor does not discretely define the boundaries of the preBötC, histological studies demonstrate that neurokinin-1 receptors are highly concentrated at the level of the preBötC (27–29). Furthermore, the application of substance P to the preBötC stimulates rhythmic network activity and excitability of synaptically isolated preBötC neurons (16, 27). The two major subclasses of substance P-responsive neurons identified in dissociated cell culture (Table S1) appeared to be preBötC neurons because they responded to neuromodulators (substance P, ATP, and norepinephrine) previously shown to modulate the activity of inspiratory preBötC neurons (16, 30–32). Additionally, both subclasses responded to histamine, and one subclass responded to bradykinin (Table S1). Constellation pharmacology correctly predicted that preBötC neurons would include both bradykinin-insensitive and -sensitive cells (Figs. 1 and 3 and Table S1). Although previous work demonstrated a role for histamine H1 receptors in stimulating breathing (33), our study demonstrates that histamine directly stimulates inspiratory preBötC neurons. The impact of bradykinin on the excitability of preBötC neurons was unknown previously. Thus, we show that constellation pharmacology, coupled with investigations in more organized network structures, can provide insight into biologically relevant cell classifications and cell-specific neuromodulation.

A comparison of bradykinin and substance P responses in dissociated cells and in the brainstem slice revealed a similar distribution of bradykinin sensitivity when normalized to the substance P response of a given cell (Fig. 3*D*). About 28% of inspiratory neurons were relatively unaffected by bradykinin (with a <20% increase in firing rate; Fig. 3*C*); this lack of response could not be predicted by firing pattern (Fig. 3*B*). The proportion of inspiratory neurons unaffected by bradykinin was expected to be larger, given that ~50% of dissociated substance P-sensitive cells were unresponsive to bradykinin (Table S1). However, it may be that not all substance-P sensitive neurons in dissociated culture are preBötC neurons.

One way in which we will explore further the cell-specific constellations of VRC neurons is through the application of subtype-selective conotoxins. We have used this strategy to identify differences in the voltage-gated Na, Ca, and K channels expressed in two different subclasses of cold- and menthol-sensitive DRG neurons (5). The ever-expanding toolkit of selective pharmacological agents, including the conotoxins among many others, will make constellation pharmacology an increasingly powerful platform for single-cell profiling. With our approach we should be able to tease apart the differential physiological roles of divergent neuronal subclasses. By combining insights at the molecular and cellular level with insights at the network level, we hope to achieve a more integrated understanding of cardiorespiratory functions, including breathing-pattern generation and modulation, thus providing a test case that bridges molecular and systems neuroscience.

Materials and Methods

Materials and methods either have been described in detail previously (5–8, 21) or are described in *SI Materials and Methods*. Transverse medullary brainstem slices were taken from male and female P7–10 mice with a C57BL/6 background as described previously (21). All procedures in this study were approved by the Institutional Animal Care and Use Committees of the University of Utah or Seattle Children's Research Institute.

ACKNOWLEDGMENTS. We thank My Huynh for assistance in preparing the figures. This work was supported by Grant GM48677 from the National Institute of General Medical Sciences.

1. Bernard A, Sorensen SA, Lein ES (2009) Shifting the paradigm: New approaches for characterizing and classifying neurons. *Curr Opin Neurobiol* 19(5):530–536.
2. Nelson SB, Sugino K, Hempel CM (2006) The problem of neuronal cell types: A physiological genomics approach. *Trends Neurosci* 29(6):339–345.
3. Franco SJ, Müller U (2013) Shaping our minds: Stem and progenitor cell diversity in the mammalian neocortex. *Neuron* 77(1):19–34.
4. Sugino K, et al. (2006) Molecular taxonomy of major neuronal classes in the adult mouse forebrain. *Nat Neurosci* 9(1):99–107.
5. Teichert RW, et al. (2012) Characterization of two neuronal subclasses through constellation pharmacology. *Proc Natl Acad Sci USA* 109(31):12758–12763.
6. Teichert RW, et al. (2012) Functional profiling of neurons through cellular neuropharmacology. *Proc Natl Acad Sci USA* 109(5):1388–1395.
7. Smith NJ, et al. (2013) Comparative functional expression of nAChR subtypes in rodent DRG neurons. *Front Cell Neurosci* 7:225.
8. Teichert RW, Memon T, Aman JW, Olivera BM (2014) Using constellation pharmacology to define comprehensively a somatosensory neuronal subclass. *Proc Natl Acad Sci USA* 111(6):2319–2324.
9. Smith JC, Ellenberger HH, Ballanyi K, Richter DW, Feldman JL (1991) Pre-Bötzinger complex: A brainstem region that may generate respiratory rhythm in mammals. *Science* 254(5032):726–729.
10. Ramirez JM, Schwarzacher SW, Pierrefiche O, Olivera BM, Richter DW (1998) Selective lesioning of the cat pre-Bötzinger complex in vivo eliminates breathing but not gasping. *J Physiol* 507(Pt 3):895–907.
11. Tan W, et al. (2008) Silencing preBötzinger complex somatostatin-expressing neurons induces persistent apnea in awake rat. *Nat Neurosci* 11(5):538–540.
12. Gray PA, et al. (2010) Developmental origin of preBötzinger complex respiratory neurons. *J Neurosci* 30(44):14883–14895.
13. Ramirez JM, et al. (2012) The cellular building blocks of breathing. *Compr Physiol* 2(4):2683–2731.
14. Gray R, Rajan AS, Radcliffe KA, Yakehiro M, Dani JA (1996) Hippocampal synaptic transmission enhanced by low concentrations of nicotine. *Nature* 383(6602):713–716.
15. Lieske SP, Thoby-Brisson M, Telgkamp P, Ramirez JM (2000) Reconfiguration of the neural network controlling multiple breathing patterns: Eupnea, sighs and gasps [see comment]. *Nat Neurosci* 3(6):600–607.
16. Peña F, Ramirez JM (2004) Substance P-mediated modulation of pacemaker properties in the mammalian respiratory network. *J Neurosci* 24(34):7549–7556.
17. Peña F, Parkis MA, Tryba AK, Ramirez JM (2004) Differential contribution of pacemaker properties to the generation of respiratory rhythms during normoxia and hypoxia. *Neuron* 43(1):105–117.
18. Zanella S, Roux JC, Viemari JC, Hilaire G (2006) Possible modulation of the mouse respiratory rhythm generator by A1/C1 neurones. *Respir Physiol Neurobiol* 153(2):126–138.
19. Dergacheva O, Griffioen KJ, Neff RA, Mendelowitz D (2010) Respiratory modulation of premotor cardiac vagal neurons in the brainstem. *Respir Physiol Neurobiol* 174(1-2):102–110.
20. Garcia AJ, 3rd, Koschnitzky JE, Dashevskiy T, Ramirez JM (2013) Cardiorespiratory coupling in health and disease. *Autonomic Neurosci* 175(1-2):26–37.
21. Ramirez JM, Quellmalz UJ, Richter DW (1996) Postnatal changes in the mammalian respiratory network as revealed by the transverse brainstem slice of mice. *J Physiol* 491(Pt 3):799–812.
22. Härtel K, et al. (2007) Calcium influx mediated by the inwardly rectifying K+ channel Kir4.1 (KCNJ10) at low external K+ concentration. *Cell Calcium* 42(3):271–280.
23. Härtel K, Schnell C, Hülsmann S (2009) Astrocytic calcium signals induced by neuromodulators via functional metabotropic receptors in the ventral respiratory group of neonatal mice. *Glia* 57(8):815–827.
24. Chen Y, Li G, Huang LY (2012) P2X7 receptors in satellite glial cells mediate high functional expression of P2X3 receptors in immature dorsal root ganglion neurons. *Mol Pain* 8:9.
25. Hone AJ, Meyer EL, McIntyre M, McIntosh JM (2012) Nicotinic acetylcholine receptors in dorsal root ganglion neurons include the alpha6beta4* subtype. *FASEB J* 26(2):917–926.
26. Whiteaker P, et al. (2007) Discovery, synthesis, and structure activity of a highly selective alpha7 nicotinic acetylcholine receptor antagonist. *Biochemistry* 46(22):6628–6638.
27. Gray PA, Rekling JC, Bocchiaro CM, Feldman JL (1999) Modulation of respiratory frequency by peptidergic input to rhythmogenic neurons in the preBötzinger complex. *Science* 286(5444):1566–1568.
28. Guyenet PG, Sevigny CP, Weston MC, Stornetta RL (2002) Neurokinin-1 receptor-expressing cells of the ventral respiratory group are functionally heterogeneous and predominantly glutamatergic. *J Neurosci* 22(9):3806–3816.
29. Pagliardini S, Ren J, Greer JJ (2003) Ontogeny of the pre-Bötzinger complex in perinatal rats. *J Neurosci* 23(29):9575–9584.
30. Doi A, Ramirez JM (2010) State-dependent interactions between excitatory neuromodulators in the neuronal control of breathing. *J Neurosci* 30(24):8251–8262.
31. Viemari JC, Garcia AJ, 3rd, Doi A, Ramirez JM (2011) Activation of alpha-2 noradrenergic receptors is critical for the generation of fictive eupnea and fictive gasping inspiratory activities in mammals in vitro. *Eur J Neurosci* 33(12):2228–2237.
32. Viemari JC, Ramirez JM (2006) Norepinephrine differentially modulates different types of respiratory pacemaker and nonpacemaker neurons. *J Neurophysiol* 95(4):2070–2082.
33. Qian ZB, Qi Y, Wu ZH (2010) [Histamine H1 receptors modulate the discharge activities of inspiratory neurons in the medial region of neonatal rat nucleus retrofacialis ex vivo]. *Nan fang yi ke da xue xue bao [Journal of Southern Medical University]* 30(1):54–56.

CHAPTER 3

NOVEL SUBCLASSES OF BRADYKININ RESPONSIVE NEURONS APPEAR IN RAT LUMBAR DORSAL ROOT GANGLIA FOLLOWING CHRONIC CONSTRICTION AND SPINAL NERVE LIGATION INJURY

Manuscript under preparation

Contributing authors:

Shrinivasan Raghuraman*, Jennifer Xie*, Mario Giacobassi, Kevin Chase, Sam Robinson, Russell W. Teichert, Frank Porreca and Baldomero M. Olivera

*These authors made equal contributions to this work.

Introduction

Remarkable advances have been made in understanding the neural circuitry that underlies pain. In addition to defining the nociceptive circuitry and identifying which neurons comprise these circuits, the cell-specific molecular changes that take place when a pathological chronic pain state is established need to be systematically elucidated. Knowing which cells change, and identifying the specific functional changes that take place in each of the relevant cell types, is a prerequisite for establishing an integrated cellular and molecular framework for chronic pain.

In this work, we demonstrate the application of constellation pharmacology (1) as a platform to monitor phenotypic changes that take place in a population of DRG neurons as a chronic pain state is established. DRG contains many different types of sensory neurons and it is of interest to observe how different cell types respond to nerve injury. The constellation pharmacology approach examines hundreds of neurons simultaneously by their individual responses to the application of different pharmacological challenges using calcium imaging. Some of the questions addressed in this work are the following: When chronic pain is established, what changes take place in the combinations of ion channels and receptors expressed in DRG neurons? How do these changes affect cellular phenotypes? Are some of these molecular changes that take place in these neurons coordinated? What molecular changes accompany the progression to neuropathic pain states?

For the present study, we have used two models of neuropathic pain: Chronic Constriction Injury (CCI) and Spinal Nerve Ligation (SNL) of the rat (2, 3). These are well-validated animal models for the chronic pain state that often follows nerve injury.

The results with the CCI and SNL rats suggest that the onset of chronic pain is accompanied by an increase in the frequency of neurons responding to bradykinin, with exaggerated effects observed in the SNL model compared to CCI. It is well known that bradykinin potently elicits pain, and there are widespread observations in the literature suggesting that bradykinin is linked in its activity to a number of ion channels and receptors expressed in sensory neurons (4). We have focused our analysis on DRG neurons that responded to the application of bradykinin. Constellation pharmacology has allowed us to observe subsets of DRG neurons that are affected by the increase in bradykinin receptor expression, and whether other changes in ion channel and receptor functions are also observed in these neurons. In addition, we performed phenotypic assessment of these bradykinin responsive neurons with the progression of neuropathic pain following day 1, 3, 6 and 14 post SNL injury.

We report a set of significant molecular changes in ATP, acetylcholine, bradykinin and capsaicin responsive neurons that result in the appearance of new subclasses of bradykinin responsive DRG neurons as a consequence of CCI and SNL injury. Some of the changes appear to occur in a concerted manner, which suggests simultaneous downstream effects of the nerve injury on the constellations of ion channels and receptors in subsets of DRG neurons. These concerted changes raise the possibility of developing a complementary combination of therapeutic drugs to prevent, reverse or inhibit the aberrant neuronal activity resulting from such concerted changes that accompany the progression to a pathological chronic pain state.

Material and methods

Animals

Adult, male Sprague-Dawley rats (200-250 g at the time of surgery, Envigo, Indianapolis, IN) were used. All procedures were performed in accordance with the guidelines of the Committee for Research and Ethical Issues of IASP under protocols approved by the University of Arizona Institutional Animal Care and Use Committee. Rats were housed three per cage on a 12 h light-dark cycle with food and water ad libitum.

Surgeries

Chronic constriction injury (CCI)

CCI surgeries were done according to the description of Bennet *et al*. (11). Briefly, rats were anesthetized with 5% isofluorane in air at 1 L/min and maintained with 2.5% isofluorane. The sciatic nerve was exposed at mid-thigh level. Four loose ligatures using 4-0 chromic gut suture were placed around the exposed sciatic nerve about 2 mm apart. Sham-operated animals underwent the same procedure but without the ligatures to the sciatic nerve. The cold allodynia and mechanical hyperalgesia of the rats was assessed before and at D14 after the surgery prior to euthanasia and tissue collection.

L5/L6 spinal nerve ligation (SNL)

The surgical procedure for L5/L6 SNL was performed according to Kim and Chung (12). Briefly, anesthesia was induced with 5% and maintained with 2.5% isofluorane in air. A 2 cm midline incision was made and the lumbar 5 and 6 spinal

nerves (L5/L6) were exposed and tightly ligated with 4-0 silk suture. The incision was closed and the animals were returned to their home cages. Sham-operated control rats were prepared in an identical manner except that the L5/L6 spinal nerves were not ligated. The tactile and thermal hypersensitivity of the rats was assessed before and at specific days after the surgery prior to euthanasia and tissue collection.

Behavioral tests

Assessment of cold allodynia and mechanical hyperalgesia

Cold allodynia was evaluated by placing rats on a metal plate maintained at 4 ºC. The frequency and accumulated duration of guarding the injured hind paw was measured for 2 min. The assessment of mechanical hyperalgesia consisted of measuring the withdrawal threshold of the paw both ipsilateral and contralateral to the site of nerve injury in response to continuously-increased pressure using a Randall Selitto apparatus (Ugo-Basile algesymeter, Stoelting, Chicago, IL) (13). A sharp withdrawal of the paw or vocalization is the end point. The paw withdrawal thresholds for each hindpaw were assessed 3 times. Cutoff was set at 500 g to avoid tissue injury. Hyperalgesia were expressed as the difference between the average ipsilateral and contralateral paw withdrawal thresholds.

Evaluation of tactile and thermal thresholds

The withdrawal threshold of the hindpaw was measured in response to probing of the plantar surface with a series of calibrated von Frey filaments (Stoelting, Wood Dale, IL) in logarithmically spaced increments ranging from 0.41 to 15 g (4–150 N). Each

filament was applied perpendicularly to the plantar surface of the left hindpaw of rats held in suspended wire-mesh cages. Withdrawal threshold was determined by sequentially increasing and decreasing the stimulus strength ("up and down" method), analyzed using a Dixon nonparametric test and expressed as the mean withdrawal threshold (14-17). The withdrawal latency of the hindpaw to an infrared radiant heat source was performed as previously described (18-20). Rats were allowed to acclimate within a Plexiglas enclosure on a clear glass plate for 30 min. An infrared heat source was directed on the glass plate underneath the plantar surface of the left hindpaw. A motion detector halted both lamp and timer when the paw was withdrawn. Baseline latencies were established around 20 s to allow a sufficient window for the detection of possible hyperalgesia. A maximal cutoff of 33 s was used to prevent tissue damage. %hypersensitivity was calculated as (baseline - post injury)/baseline x 100%.

Statistical analysis

All results were expressed as mean ± SEM. Statistical analyses were calculated using GraphPad Prism 7 software. An unpaired t-test (two-tailed) was used when only two groups were compared; the t and P values are reported in the Results section. For three or more group comparisons, a One-Way ANOVA post-hoc Tukey's multiple comparisons test was used for between-group comparisons. The F(DFn,DFd) and P values are reported for the ANOVA tests; post hoc comparison is reported as "significant" or not without the actual P value. $P<0.05$ was identified as significant.

DRG cell culture

Two weeks after the surgeries, the lumbar DRG of all animals were dissected. For CCI trials, DRG from L4, L5 and L6 were pooled from both the ipsilateral and contralateral side of both experimental and sham-operated control animals. For SNL trials, L5and L6 DRGs were pooled from both the ipsilateral and contralateral side of both experimental and sham-operated control animals, while L4 DRG was cultured separately. The pain state of the animals was assessed by monitoring cold allodynia. The tissues were stored separately in cell culture medium and shipped on ice overnight. DRG fragments were kept on ice, transferred to a tissue culture-treated (by vacuum gas plasma) Petri dish (BD Biosciences) with HBSS (ThermoFisher, cat# 14175103) and cleaned to remove debris and excessive tissue. The DRGs were chopped using spring scissors and transferred with a large-diameter fire-polished Pasteur pipette to a 15-mL conical tube. The total volume was adjusted to 900 μL with HBSS; 100 μL 2.5% (wt/vol) trypsin were added (for a working concentration of 0.25% (wt/vol) trypsin), and the tube was incubated at 37 °C in a water bath for 18 min. The contents of the tube were mixed three or four times during the trypsin incubation by gently flicking the tube. After incubation, the DRG neurons were washed three times with 4 mL cell culture medium. Each wash was performed by adding 4 mL cell culture medium, allowing DRGs to settle to the bottom of the tube and removing as much medium as possible with a fire-polished Pasteur pipette without removing any DRGs. After the final wash, DRGs were resuspended in 1.5 mL cell culture medium. The DRG suspension was triturated 5–10 times (or until there was no resistance) through a series of fire-polished pipettes, where each successive pipette had a smaller tip diameter. The solution became cloudy as

individual neurons dissociated from the ganglia. Any undissociated tissue was carefully removed using a Pasteur pipette. The suspension was centrifuged at 50 X g for 10 min. After centrifugation of the cell suspension, the supernatant was removed by aspiration, leaving behind the volume of medium required to plate dissociated DRG neurons, typically into two wells (40μL total). Neurons were resuspended in the remaining medium by gentle trituration with a 200-μL disposable plastic pipette tip. In general, 3 DRG ganglia tissue (L4, L5, L6 from one side of an animal) yielded a 40uL volume of cell suspension that was plated in two wells.

Plating cells

Silicone rings were cut with cork borers from 0.25-mm-thick silicone sheets (Grace BioLabs). Each ring had an outer diameter of ~10 mm and an inner diameter of ~3 mm. The rings were washed sequentially with 70% (vol/vol) ethanol and deionized, filtered water, 100% ethanol and 70% ethanol and dried. Each silicone ring was placed on the floor of a well of a poly-D-lysine–coated 24-well tissue culture plate (BD Biosciences) and sealed to the floor with gentle pressure applied with the tips of a pair of dull forceps.

20 μL cell suspension was added to the center of each silicone ring of the multi-well plate and the plates were placed in the 37 °C incubator for 45–60 min to allow cells to settle and adhere. After 60 min, 1mL cell culture medium was added and the plates were placed in a 37 °C, 5% CO_2 tissue culture incubator, and the cultures were used for imaging after 18–36 h.

Loading cells with Fura-2-AM and calcium imaging

After culturing overnight, the 24-well plate was placed in a sterile tissue culture hood; 1 mL culture medium in each well was agitated by pipetting it up and down vigorously in the well to suspend all dead cells and dislodge any cells that were only loosely adherent.

The medium was replaced with 500 μL fresh cell culture medium containing 2.5 μM Fura-2-AM, which was freshly prepared by thawing the single-use stock aliquot of 1 mM Fura-2-AM (ThermoFIsher, cat# F-1221) in DMSO and adding it to cell culture medium followed by vigorous vortexing for ~20 s. The plate was placed in the 37 °C incubator for 1 h, after which the medium was replaced with 1 mL fresh MEM + supplements, and the plate of cells was allowed to equilibrate to room temperature for 20 min. Just before imaging a particular well, the MEM + supplements solution in the well was replaced with observation solution. The observation solution was replaced two additional times to completely remove free Fura-2-AM.

Digital video microscopy

All images were obtained with a 10x objective on an inverted microscope (Nikon Eclipse Ti-U). A Sutter Instruments Lambda DG light source (300-W Xenon arc lamp) fitted with a filter wheel was used as the source of excitation light at 380 and 340 nm. Images were acquired with an Andor Zyla sCMOS camera and Nikon NIS elements software.

After loading with Fura-2-AM, a 24-well plate was fastened to the microscope stage. A bright-field image of a single field of view was captured and used to select

regions of interest (ROIs) corresponding to the area (delineated by the outer perimeter) of all nonoverlapping cells in the field. Each ROI, corresponding to a single cell, was monitored for $[Ca^{2+}]_i$. Typically, >100 neurons were imaged for each experiment. The fluorescence emission was monitored at 510 nm for both 380- and 340-nm excitation. The exposure time was adjusted for each experiment to a maximum ROI intensity of ~3,500 gray levels for 380-nm excitation and ~1,000 gray levels for 340-nm excitation. An image was captured at each excitation wavelength, and the ratio of fluorescence intensities at excitation wavelengths of 340 and 380 nm was acquired one time every 1 or 2 s to monitor the relative changes in calcium concentration in each cell as a function of time. Nikon NIS elements software generated a calcium response profile in the form of a trace with 340/380 nm ratios on the y-axis and time on the x-axis.

Preparation of solutions

Cell culture medium

The medium for culturing dorsal-root ganglion (DRG) neurons was minimal essential media MEM (Invitrogen) supplemented with 10% (vol/vol) FBS (Hy-Clone) penicillin (100 U/mL), streptomycin (100 μg/mL), 1X Glutamax (Invitrogen), 10 mM Hepes and 0.4% (wt/vol) glucose. The medium was adjusted to a pH of 7.4 with NaOH, filtered through a 0.22-μm filter under sterile conditions and stored at 4 °C until shortly before use, when it was allowed to warm to 37 °C in a tissue culture incubator with 5% CO_2 atmosphere.

DRG observation solution

The observation solution for calcium-imaging and immunostaining experiments consisted of 145 mM NaCl, 5 mM KCl, 2 mM CaCl2, 1 mM MgCl2, 1 mM sodium citrate, 10 mM Hepes and 10 mM glucose. A 10X stock of observation solution (but without sodium citrate or glucose) was prepared with penicillin streptomycin at 100 U/mL and 100 µg/mL, respectively, and stored at 4 °C. No additional penicillin streptomycin was added to the 1X observation solution. Sodium citrate and glucose were added to the 1X solution to yield their final concentrations given above. The final solution was adjusted to a pH of 7.4 with NaOH, and stored at 4 °C until used.

For membrane depolarization by high extracellular potassium, $[K^+]_o$, 30 mM $[K^+]_o$ in DRG observation solution was made from a stock of 100 mM high K+ solution. A stock of 100 mM high K+ solution was made by adding 50 mM NaCl, 100 mM KCl, 2 mM CaCl2, 1 mM MgCl2, 1 mM sodium citrate, 10 mM Hepes, 10 mM glucose and 1mL 10X penicillin-streptomycin, adjusted to a pH of 7.4 with NaOH and stored at 4 °C until used. The osmolarity of this stock solution is equivalent to that of DRG observation solution because an equimolar concentration of NaCl is replaced by KCl.

Ligand concentrations

All stock solutions of ligands for calcium-imaging were stored at −20 °C in small-volume aliquots to avoid repetitive freezing and thawing, with the exception of allyl isothiocyanate, which was stored at 4 °C. All working concentrations were obtained by diluting stock solutions into DRG observation solution. Stocks were 1 M acetylcholine (Sigma cat# A6625) in water, 10 mM adenosine triphosphate (Sigma cat# FLAAS-1VL)

in water, 2 mM bradykinin (Tocris, cat# 3004) in water, 640 mM (1R, 2S, 5R)-(-)-menthol (Sigma, cat# M2780) in ethanol, allyl isothiocyanate (mustard oil) (Sigma-Aldrich) was purchased as a 10.2 M solution, 20 mM capsaicin (MP Biomedicals) in DMSO.

Experimental protocol

Calcium signals were elicited by a ~15-s application of various ligands in DRG observation solution. The observation solution was aspirated from the well with a peristaltic pump controlled by a foot pedal, and observation solution containing a working concentration of ligand was applied manually at the edge of the well from a 1mL pipette tip. After 15 s, the ligand solution was replaced completely with observation solution in the same manner. After an additional 40 s and 1 min after the application of ligand, the observation solution was replaced with a second and third aliquot of observation solution, respectively. This procedure was repeated as necessary, generally at 5-min intervals for various ligands. The order of ligand application was chosen such that the more hydrophobic and less reversible ligands were applied towards the end (such as AITC and capsaicin) and reversible ligands were applied towards the beginning of an experiment.

After the video microscopy protocols, cells were stained with Alex-568–labeled isolectin B4 (IB4) (ThermoFisher cat# I21412) at a concentration of 2.5 μg/mL in DRG observation solution for >5 min followed by three washes with DRG observation solution over a period of 3 min.

Immunostaining

After the experiments were performed on all wells, the 24-well plate was removed from the microscope stage. DRG observation solution was aspirated and washed with ice-cold DRG observation solution 2 times. The cells were fixed with 4% ice-cold paraformaldehyde in PBS for 30 min at room temperature on a shaker. After 30 min, paraformaldehyde was aspirated and cells were washed 3 times with ice-cold DRG observation solution. Cells were permeabilized with 0.25% Triton X-100 in DRG observation solution for 30 min at room temperature on a shaker. After the permeabilization step, cells were washed 3 times with ice-cold DRG observation solution and were treated with a blocking buffer for 30 min at room temperature on a shaker. The blocking buffer consisted of 10% normal donkey serum (Jackson Immunoresearch cat # 017-000-121) in DRG observation solution and 30 mM glycine. The cells were washed 2 times with ice-cold DRG observation solution. 1 mL of anti-CGRP primary antibody (1:2000 dilution, Immunostar cat# 24112) in 0.1% donkey serum was added to the wells and the cells were incubated with primary antibody overnight at 4 ^{o}C on a shaker. The primary antibody was aspirated and cells were washed 3 times with ice-cold DRG observation solution. 1 mL secondary antibody (1:200 dilution, Thermofisher cat#A-21206) in DRG observation solution was added and cells were incubated with secondary antibody for 1 h at room temperature on a shaker. The cells were washed with DRG observation solution 3 times. Bright field and fluorescent images were taken on the microscope. To identify the same field of view, previously created ROIs were overlayed with the bright field image.

Data analysis

The time course of the 340:380 ratio for each ROI (trace) was analyzed using a set of R functions (R Core Team 2013) for quantitative analysis of peak heights, clustering and determination of cell-phenotype percentages as described previously (5). Neuronal cell populations were compared using a logistic regression of binary response score onto population type nested within experiment date. To compare ipsilateral CCI neurons to contralateral CCI neurons, the glm function of R was used as: glm(bin ~ ipsi/date, family="binomial") where bin is a response indicator (0,1), ipsi is 1 for neurons from the ipsilateral CCI and 0 for neurons from the contralateral CCI, and date is the date of the experiment.

The responses to the application of ligands were also scored manually in a binary format (0 or 1 for absence and increase of calcium influx, respectively). The baseline calcium level for each cell trace was observed and a response was assigned as positive calcium influx (value=1), if the magnitude of calcium influx was higher than a threshold of 0.05 units (of 340/380 ratio) above the baseline. In rare cases where the calcium response to the application of previous ligand did not return to baseline, a mild deflection of calcium signal was assessed to call for a positive a response. In general, a 5 min or 7 min interval between applications was used to obtain a fully reversible calcium profile.

Results

Behavioral studies following CCI and SNL nerve injury

Figure 3.1 shows the behavioral assays performed on rats following CCI and SNL nerve injury. As shown in Figure 3.1A, the rats display higher sensitivity to cold with

increased frequency of paw withdrawal (Figure 3.1A) and increased duration of withdrawal events (Figure 3.1B) following CCI injury. In SNL injured rats, thermal and mechanical hypersensitivity were observed following injury. The threshold to thermal stimulus reduced in injured rats compared to the baseline scores monitored before the injury, and to sham-operated rats (Figure 3.1C). Similarly, the withdrawal threshold to mechanical sensitivity also decreased significantly compared to scores before injury and to sham operated animals (Figure 3.1D), ($p<0.05$ for all behavioral studies).

Changes in membrane receptor compositions of DRG neurons following CCI and SNL injury

A primary culture of dissociated DRG cells was prepared and analyzed using constellation pharmacology. Seven pharmacological challenges were given (indicated by the arrows) and examples of responses from individual neurons are shown in each trace. A peak signifies an increase in cytosolic calcium concentration, $[Ca]_i$, in response to the pharmacological challenge. Each specific pharmacological challenge may or may not elicit a transient increase in calcium as monitored by fluorescence of the calcium-sensitive dye Fura 2 using two wavelengths. In the experiments shown, examples of the diverse responses of individual neurons in the same well are illustrated for both the control contralateral DRG cultures and the ipsilateral DRG cultures from the CCI and SNL animals.

The responses to the application of 30 mM $[K^+]_o$ was used to differentiate neurons from non-neuronal cells. In addition to responses elicited by $[K^+]_o$, the diversity of response patterns to six pharmacological challenges is quantitated in Table 3.1. For CCI

trials, DRG neurons from 13 CCI operated rats and 11 sham-operated rats were analyzed and for SNL trials, neurons from 5 SNL operated and 4 sham operated rats were analyzed. Although there is some variation in the three uninjured DRG groups (contralateral CCI and ipsilateral and contralateral DRG from sham-operated animals), the data reveal a significant divergence in the frequency of cells responding to the pharmacological challenges in the ipsilateral CCI DRG neurons (Table 3.1). Figure 3.2 summarizes these molecular changes following CCI and SNL injury. As shown in Figure 3.2A, there was a *decrease* in the frequency of neurons responding to acetylcholine ($p<0.05$) and capsaicin ($p<0.001$) in the ipsilateral CCI, and a significant *increase* in the frequency of neurons responding to ATP and bradykinin ($p<0.001$). These observations align with previous studies performed on whole DRG (6-8). These differences were extensively upregulated in SNL operated rats as shown in Figure 3.2B. We have specifically investigated the increase in the frequency of DRG neurons that respond to bradykinin in the injured ipsilateral DRG neurons of the CCI- and SNL-operated rats.

For the ease of understanding these data sets, we have grouped data obtained from uninjured DRG neurons (contralateral CCI, sham-operated ipsilateral and contralateral DRG neurons) and labeled them as “CCI controls” and similarly grouped data obtained from uninjured DRG neurons from SNL-operated and sham-operated rats (SNL ipsilateral L4, SNL contralateral L4, SNL contralateral L5L6, sham-operated ipsilateral and contralateral L4, L5 and L6) and labeled them as “SNL control”. As noted in Table 3.1, there were no differences observed between uninjured DRG neurons in their responsiveness to the panel of pharmacological agents tested.

Assessing the behavioral changes with the progression of neuropathic pain

We performed behavioral assays and constellation pharmacology experiments on injured DRGs at different time points following SNL injury to identify the behavioral and molecular changes with the progression of pain states. As shown in Figure 3.3A, the SNL-injured rats display progressive reduction in thresholds to mechanical stimulus (Figure 3.3A) and heat stimulus (Figure 3.3B) starting at 3, 6 and 14-day post SNL injury. These scores were compared with sham-operated rats and baseline scores prior to nerve injury. As shown in Figure 3.3, rats do not display any allodynia on Day 1, but begin to develop tactile allodynia ($p<0.05$) and thermal hyperalgesia ($p<0.001$) on Day 3 following injury.

Tracking molecular changes with the progression to neuropathic pain states

To identify the earliest molecular changes that appear following nerve injury, SNL injured rats were behaviorally monitored at Day 1, 3, 6 and 14 after injury as shown in Figure 3.4. The acetylcholine responsive neurons significantly reduced in SNL-injured DRG at Day 1 (11%± 2% of the total neurons, $p<0.001$) compared to controls (33% ± 4% of total neurons). In addition, there was a significant increase in ATP responsive neurons (75% ± 2% of total neurons, $p<0.001$) in SNL-injured DRG at Day 1 compared to controls (44%± 4% of the total neurons). Capsaicin responsive neurons began to reduce starting Day 3 and continued to decrease until Day 14. Progressive increase in bradykinin responsive neurons were observed at Day 3, 6 and 14 as shown in Figure 3.4. Thus, we

monitored the molecular changes that appeared with the progression of pain states and the resulting effects in bradykinin responsive neuronal phenotypes.

Grouping DRG neurons based on phenotypic calcium profiles

In the experiments summarized in Figure 3.2, the frequency of neurons responding to bradykinin in all of the control groups was similar (~12% ± 2%). In contrast, the frequency of bradykinin responsive neurons obtained from injured DRG were approximately two-fold higher in ipsilateral CCI (34% ± 2%) and five-fold higher in ipsilateral SNL L5L6 (66% ± 2%). Although the frequency of cells responding to bradykinin varied from experiment to experiment, the ipsilateral DRG neurons from CCI and SNL consistently showed a significant increase ($p<0.001$) compared to contralateral DRG neurons in all experiments on animals that displayed chronic pain states in behavioral assays.

An alternative analysis of the data is to classify subsets of cells that have a particular pharmacological profile as shown in Figure 3.5. The bradykinin responsive neurons were categorized in 5 groups based on their responses to the application of other pharmacological agents and their frequency of appearance is summarized in Figure 3.6. Group 1 neurons, in addition to responding to bradykinin, also respond to both menthol and capsaicin. Furthermore, the response of these neurons to AITC is very robust. In contrast, Group 2 neurons do not respond to menthol, but uniformly respond to capsaicin. There is heterogeneity in their response to AITC, but the response is not robust, if it occurs. These two groups appear to be canonical bradykinin responsive neurons and they were observed in all cell cultures as indicated in Figure 3.6. Groups 3-5 neurons were

absent in control cultures from CCI and SNL and appeared only in injured DRG (ipsilateral CCI and ipsilateral SNL L5L6). Thus, the appearance of three new phenotypic groups of bradykinin responsive neurons with distinctive pharmacological profiles contributed towards the majority of increase in bradykinin responses show in Figure 3.2. Group 3 neurons responded to ATP and bradykinin only and contributed towards 11% increase in bradykinin responses from ipsilateral CCI culture and 30% increase in ipsilateral SNL L5L6 (shown in Figure 3.6A). Group 4 neurons were defined based on their magnitude of response to acetylcholine and ATP. In this group, the magnitude of ATP responses was higher than acetylcholine and they generally responded to the application of AITC. Similar to group 3, these neurons appeared only in ipsilateral CCI and SNL L5L6 and were absent in all controls. The pharmacological profile of Group 5 is a hybrid between Groups 3 and 4. Unlike Group 4 neurons, these did not respond to acetylcholine, but like Group 4 neurons, responded to ATP and to AITC. They differ from the Group 3 neurons that uniformly did not respond to the application of AITC.

There were additional (~8%) bradykinin responsive neurons that appeared in SNL ipsilateral L5L6 cultures in addition to the five groups described above and these have not been grouped as they require more detailed analysis. Thus, Group 1 and 2 are more canonical neurons that may include polymodal peptidergic nociceptors found in controls, ipsilateral CCI and ipsilateral SNL L5L6. The CCI and SNL injury result in the appearance of three new groups that are shown in Figure 3.5 (Group#3- 5).

In addition, the incremental increase in bradykinin responsive neurons that was observed at 3, 6 and 14 days post injury (Figure 3.4) were phenotypically assessed and the progressive increase in bradykinin responses appeared from the new cellular

phenotypes described above (Figure 3.5, Group# 3-5). The quantitative analysis of these phenotypes, as shown in Figure 3.6B, demonstrate that the new bradykinin responsive neurons are absent at Day 1 following injury and begin to appear and increase starting Day 3 post injury.

Coordinated changes in three different receptors based on
the magnitude of responses to ligand application

In addition to the frequency of responses, the magnitudes of calcium responses were assessed. An example of coordinated changes associated with the increased responsiveness to bradykinin emerged through the analysis of the neurons that responded to both ATP and acetylcholine (Figure 3.7). Figure 3.7A shows phenotypic calcium-imaging traces of neurons from ipsilateral CCI DRGs that were responsive to both acetylcholine and ATP. Figure 3.7C shows similar traces from ipsilateral SNL DRGs. These have been sorted further into two groups: those that also responded to bradykinin and those that did not. We observed that in the neurons that express the bradykinin receptor, the calcium transient in response to ATP was generally greater than the calcium transient in response to acetylcholine. However, in the class of neurons that did not respond to bradykinin, the converse was usually true. This relationship is illustrated using a log plot as shown in Figure 3.7B and Figure 3.7D. The plot shows the logarithm of the ratio of the magnitude of responses of acetylcholine to ATP in each cell. In the controls, the responses to acetylcholine are commonly greater than the responses to ATP. In addition, the plot demonstrates that there is a leftward shift of the curve associated with ipsilateral CCI, suggesting that a significant proportion of neurons that responded to both

acetylcholine and ATP now exhibit a larger magnitude of response to ATP than to acetylcholine. This effect is more pronounced in ipsilateral SNL cultures, as shown in Figure 3.7D. In contralateral CCI, 28% percent of these neurons (grey arrow) had higher ATP magnitude than acetylcholine and the majority of neurons (72%) had higher magnitude of acetylcholine than ATP. In ipsilateral CCI, an increased percentage of neurons (39%) had an ATP response magnitude that was greater than acetylcholine and the majority of these neurons were responsive to bradykinin. Thus, in the cluster of neurons represented to the left of the vertical line in Figure 3.7B, there are coordinated changes compared to the controls: (1) the response to ATP became greater than the response to acetylcholine (not observed in most control neurons), and (2) a high proportion of neurons with an acetylcholine/ATP response <1 became responsive to bradykinin. Thus, the constellation of functional ion channels and receptors was altered in three different receptors and ion channels to yield the distinctive pharmacological profile found in a subset of ipsilateral DRG neurons.

In SNL cultures, the same trends were also evident and more pronounced. Only 29% of the neurons had acetylcholine responses greater than ATP responses, whereas in contralateral SNL cultures, 93% of the neurons had a phenotype where ACh magnitude was greater than ATP magnitude. Thus, DRG neurons from ipsilateral SNL exhibit profound concerted changes in receptor expression: significant upregulation of ATP receptors and downregulation of ACh receptors, accompanied by new expression of bradykinin receptors in the same neurons.

Effects of nerve injury on IB4 and CGRP stains

The cells were stained with isolectin B4 (shown in red, IB4 conjugated with Alexa 564 dye) to identify non-peptidergic nociceptors and an antibody for CGRP (shown in green, secondary antibody conjugated with Alexa 488 dye) to identify peptidergic nociceptors. In neurons subjected to CCI, the percentages of IB4 and CGRP stained neurons were reduced and nearly absent in ipsilateral SNL cultures, as shown in Figure 3.8. The bradykinin responsive cell groups were analyzed for these stains. Group 1 and Group 2 neurons were largely positive for CGRP in controls. In contrast, the new cell groups that appear in ipsilateral CCI and ipsilateral SNL L5L6 cultures (Groups 3-5, Figure 3.5) were negative to both IB4 and CGRP stains. These staining data suggest that multivalent molecular changes occur in different cell types (unlabeled cell, IB4+cells and GCRP+ cells) that result in convergence to new bradykinin responsive neuronal phenotypes. It is also notable that the majority of the $IB4^-$ $CGRP^-$ neurons in control DRG were capsaicin responsive, and a significant fraction of these cells did not respond to capsaicin in the ipsilateral CCI and SNL L5L6 DRG. These results are suggestive of coordinated, multivalent changes in ATP, bradykinin and capsaicin receptors in a subset of DRG neurons that could result in the appearance of new bradykinin responsive neuronal phenotypes.

Discussion

We analyzed functional phenotypic changes that occur in DRG neurons when a pathological chronic pain state is established after CCI and SNL. Neurons from the ipsilateral lumbar DRG from CCI and SNL were compared to multiple controls,

including neurons from the contralateral DRGs of the same animal and from ipsilateral and contralateral DRGs from sham-operated animals. There were no significant differences observed between the three control DRG cultures. In contrast, significant differences were detected between neurons from ipsilateral DRG of CCI/SNL rats and controls.

One of the most notable observations was the increase in the fraction of DRG neurons that responded to bradykinin (Figure 3.2). The increase in the number of DRG neurons expressing these receptors can be accounted for by three distinctive neuronal subclasses, as described in Figure 3.5. One neuronal subclass responded to bradykinin and ATP. The DRG neurons that share this profile accounted for approximately half of the observed increase in the overall frequency of neurons responding to bradykinin (Figure 3.6A).

Another subset of neurons expressed bradykinin receptors with a distinctive pharmacological profile found only in the injured ipsilateral CCI and SNL DRG, and not the uninjured control DRGs that also responded to ATP and acetylcholine as is illustrated in Figure 3.7. In controls, the neurons that responded to both acetylcholine and ATP mostly exhibited a greater response to ACh than to ATP. A significant fraction of all neurons that responded to both compounds in the injured DRG trials exhibited a relative increase in the response magnitude to ATP, and a relative decrease in the response magnitude to acetylcholine (demonstrated by the left-shifted segment of the red curve in Figure 3.7B and Figure 3.7D). The detailed phenotypic response of these cells is shown by the last two traces displayed in Figure 3.7A: a profile found in the ipsilateral DRG

cultures from CCI- and SNL-operated animals and absent in the controls, suggesting a concerted molecular interplay between acetylcholine, ATP and bradykinin receptors.

In addition, another example of coordinated changes was observed in capsaicin responsive neurons. The extreme downregulation of capsaicin responsive neurons suggests that TRPV1 expression is decreased following CCI and SNL injury. It is unclear how the reduction in TRPV1 could lead to pain states as TRPV1 has been conventionally associated with nociception, although TRPV1 receptor itself may not mediate pain signal (9). Nevertheless, this observation requires investigation of constellations of other receptors within the TRPV1 expressing neurons that could provide hints on how these combinatorial changes result in a physiologically relevant neuropathic pain state.

A third subset of neurons with a pharmacological profile found only in the experimental neurons (from ipsilateral DRGs in CCI and SNL rats) is illustrated in Figure 3.5 as the Group #5. These neuronal phenotypes appear to represent a subset of the Group 4 neurons that have lost their responsiveness to ACh completely. Together, Groups 3, 4 and 5 account for the majority of increase in the frequency of DRG neurons that respond to bradykinin in the ipsilateral CCI and SNL DRGs, are only found in injured DRG and were absent in uninjured DRG.

In addition to changes in receptor compositions, we also observed decrease in the expression of CGRP and binding of IB4. These changes in neurons from injured DRG (ipsilateral CCI and SNL) suggests two hypotheses: 1) once pain state is established, previously non-nociceptive neurons begin to express markers of nociceptive neurons, such as upregulated expression of bradykinin and ATP receptors, and/or 2) the properties of nociceptive neurons change by losing IB4 binding and/or CGRP expression in addition

to the many changes in receptor and ion channel expression. Together, these changes could result in the appearance of new phenotypic neuronal groups as shown in Figure 3.5 (Group#3-5).

To monitor the earliest molecular events that occur following nerve injury, we performed a series of experiments at Day 1, 3, 6 and 14 following SNL injury. As shown in Figure 3.3, the behavioral tests to assess the thresholds for tactile and thermal sensitivity reduced starting Day 3. The corresponding molecular changes are shown in Figure 3.4. As shown, at Day 1 following nerve injury, the pain scores of animals tested were similar to sham-operated rats but some molecular changes already began to appear in DRG with a decrease in ACh responsive neurons and an increase in ATP responsive neurons. This suggests that changes in ACh- and ATP-responsive neurons are necessary, but not sufficient to establish neuropathic pain. The decrease in behavioral thresholds correlated with increase in bradykinin responsive neurons and suggests that coordinated changes in ACh, ATP, bradykinin, and capsaicin are required to result in neuropathic pain. These coordinated changes are phenotypically examined and illustrated in Figure 3.5 and Figure 3.7.

Two questions that arise are: does the appearance of these new phenotypes contribute towards neuropathic pain or do these phenotypes appear as a result of nerve injury? These questions require further investigation like 1) testing pharmacological interventions that alleviate chronic pain and observing their effects on the appearance of these aberrant neuronal phenotypes 2) using a cocktail of pharmacological blockers of ATP and bradykinin receptors and observe its effect on rat behavior following nerve injury. Thus, the current work opens new avenues to explore chronic pain studies at

cellular and molecular levels. In this study, we have defined a set of functional changes in receptor and ion channel expression that result in appearance of new neuronal phenotypes using constellation pharmacology, demonstrating that this approach can be used to monitor cellular and molecular changes in pathological states in other animal models of disease, even when genetic tools are not readily available.

In addition, the novelty of these experiments is demonstrated by tracking the coordinated changes in membrane constellations within individual neurons, as opposed to studying the global transcriptional changes in whole population of DRGs where cell-specific changes and functional changes are unknown. Among other implications, this approach paves the way to a new paradigm of identifying drugs that could focus on reducing/preventing the progression of neuronal cell types to the three new bradykinin responsive cell groups described in this study.

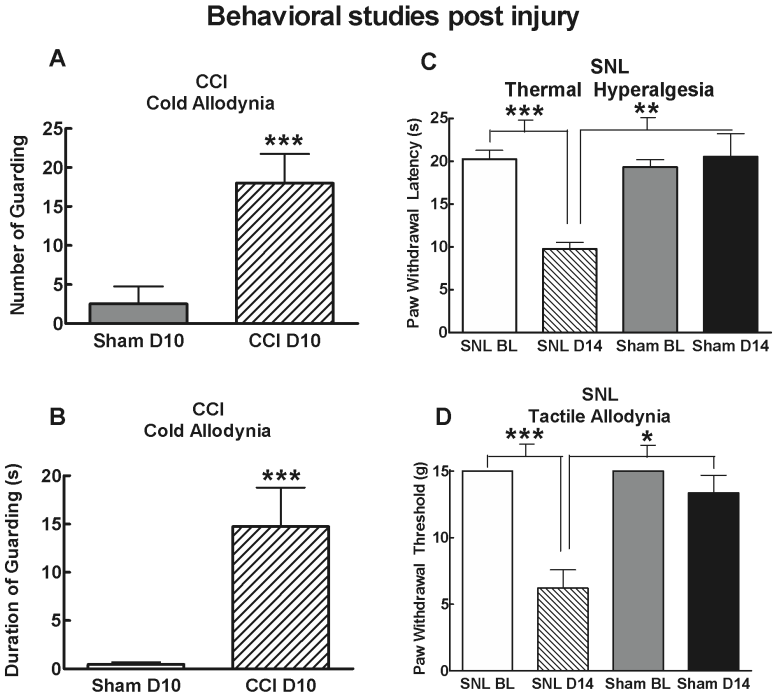

Figure 3.1: Summary of behavioral assays performed on rats subjected to CCI and SNL injury

A shows the number of times rats lifted their paws (number of guarding events). **B** shows the duration of guarding events in response to cold plate assay performed after CCI injury. A and B show that the CCI-operated rats had significantly higher number of guarding events and guard duration compared to sham-operated rats. **C** indicates the threshold to lift paw in response to heat stimulus. **D** indicates the threshold to respond to mechanical stimulus to injured paw after SNL injury. As shown, the SNL injured rats show thermal and mechanical hypersensitivity following SNL injury. For CCI, behavioral experiments were performed 10 days after injury. For SNL, behavioral experiments were performed 14 days after injury. SNL injured animals were tested before and after surgery. SNL BL: Baseline score obtained from animal before SNL surgery, SNL D14: 14-days post SNL surgery, Sham BL: Base line score obtained from sham-operated animal before surgery, Sham D14: Sham-operated animals 14-days post-surgery. For CCI, n=13 rats and 11 sham-operated rats; For SNL n=5 SNL-operated and 5 sham-operated rats. *=$p<0.05$, **=$p<0.01$, ***=$p<0.001$.

Figure 3.2: Summary of profiling experiments from CCI and SNL injured DRG neurons 14-days after injury

The plots show the average percentage of neurons that responded to the applications of pharmacological ligands. ACh: 1mM acetylcholine, ATP: 20uM ATP, BR: 10uM bradykinin, ME: 400uM Menthol, AITC: 100uM allyl isothiocyanate, C: 500nM capsaicin. **A** compares neurons from injured CCI DRG with uninjured DRG neurons and the percentage of ATP and bradykinin responsive neurons are significantly higher compared to controls (explained in main text), whereas the percentage of acetylcholine- and capsaicin-responsive neurons were decreased. The number of neurons and number of trials compared are: ipsilateral CCI= 5035 neurons from 33 trials, contralateral CCI=4519 neurons from 29 trials, ipsilateral sham=2176 neurons from 21 trials, contralateral sham=2028 neurons from 17 trials. The data were obtained from 13 CCI-operated and 11 sham-operated rats. *=$p<0.05$, **=$p<0.01$, ***=$p<0.001$

B summarizes the average percentage of neurons that responded to the application of pharmacological ligands in SNL injured DRG compared to uninjured DRGs. The neurons responsive to bradykinin and ATP were significantly increased after SNL injury, and the acetylcholine- and capsaicin-responsive neurons were significantly lower compared to uninjured DRG neurons. The number of neurons and trials compared were: ipsilateral SNL L5L6= 1028 neurons from 5 trials, contralateral SNL L5L6= 960 neurons from 5 trials, sham ipsilateral L5L6= 714 neurons from 4 trials, sham contralateral L5L6 = 277 neurons from 2 trials. The data were obtained from 5 SNL-operated rats and 4 sham-operated rats. *=$p<0.05$, **=$p<0.01$, ***=$p<0.001$

A

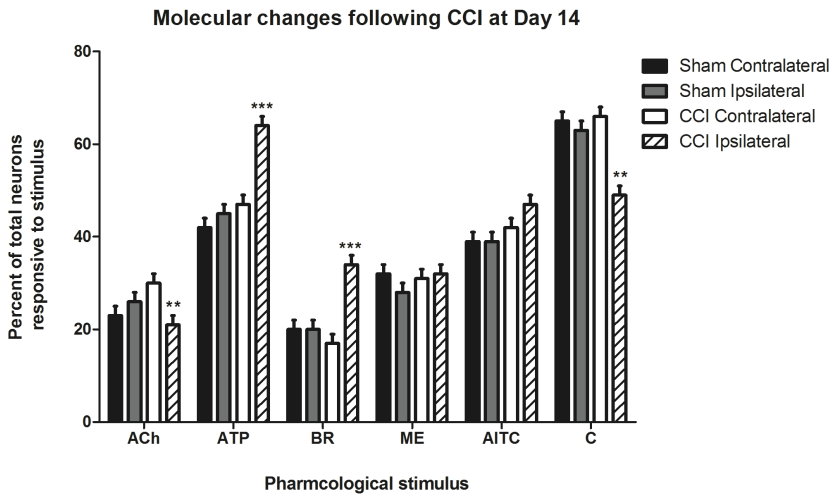
Molecular changes following CCI at Day 14
Sham Contralateral
Sham Ipsilateral
CCI Contralateral
CCI Ipsilateral
Percent of total neurons responsive to stimulus
0
20
40
60
80
**
***
***
**
ACh
ATP
BR
ME
AITC
C
Pharmcological stimulus

B

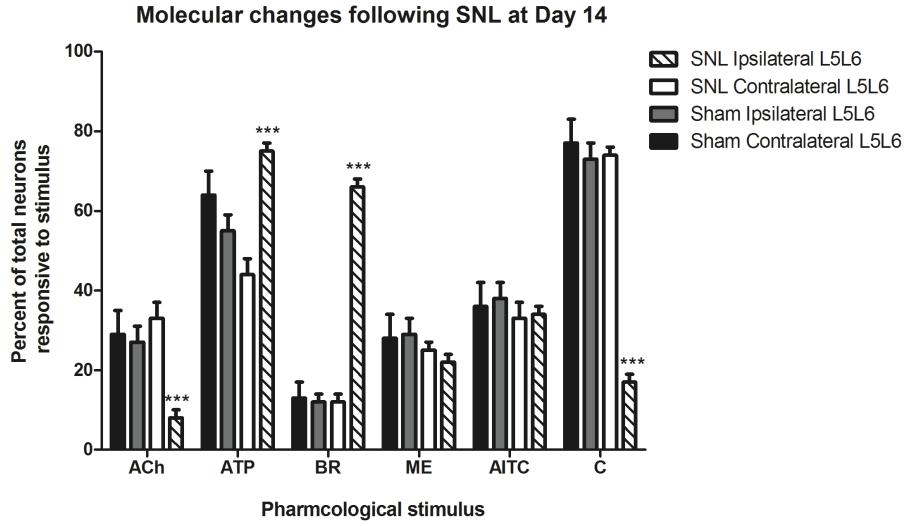
Molecular changes following SNL at Day 14
SNL Ipsilateral L5L6
SNL Contralateral L5L6
Sham Ipsilateral L5L6
Sham Contralateral L5L6
Percent of total neurons responsive to stimulus
0
20
40
60
80
100
***
***
***
***
ACh
ATP
BR
ME
AITC
C
Pharmcological stimulus

A

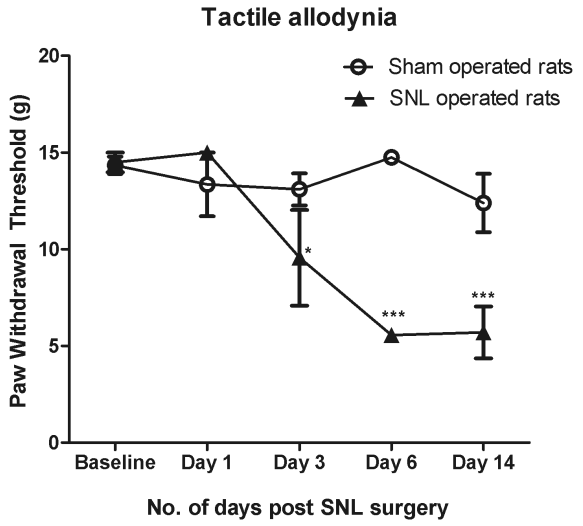

B

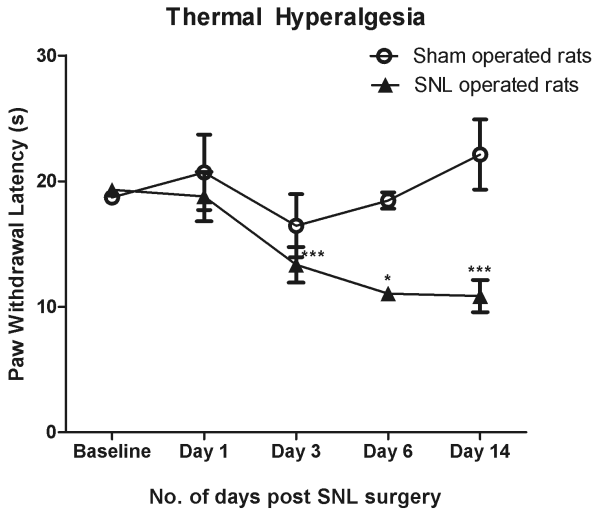

Figure 3.3: Monitoring the progression of pain behaviors due to SNL injury
The panels show the behavioral test scores obtained for SNL injured rats after 1, 3, 6 and 14-days post-surgery compared with sham-operated rats. **A** compares tactile sensitivity and **B** compares thresholds for thermal sensitivity of SNL injured rats with sham-operated rats. As shown, the threshold for tactile and thermal stimulus gradually decreases starting Day 3 post-surgery. *=$p<0.05$, **=$p<0.01$, ***=$p<0.001$

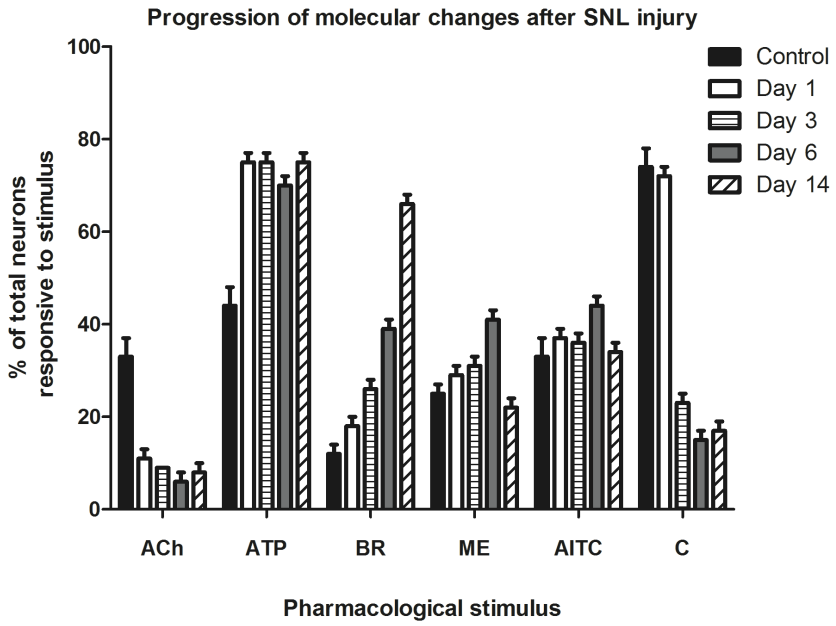

Figure 3.4: Monitoring molecular changes with the progression of neuropathic pain induced by SNL injury. SNL injury induced molecular changes at Day 1, 3, 6 and 14 after injury. The earliest changes were observed in the frequency of neurons responsive to acetylcholine and ATP. Only 11%±2% of total neurons obtained from injured DRG were responsive to ACh compared to 33%±4% in uninjured DRGs (controls) on Day 1 following SNL injury. The bradykinin responsive neurons progressively increased starting Day 3 and significantly increased to 66%±4% at Day 14 post SNL injury.

Figure 3.5: New bradykinin responsive neuronal phenotypes appear following CCI and SNL injury. The bradykinin responsive neurons were categorized into 5 phenotypic groups based on their calcium response phenotypes to the application of pharmacological ligands. Each calcium-imaging trace is a representative response profile from a single neuron within the group. Group 1 and Group 2 are bradykinin responsive neurons that responded to capsaicin. Group 1 neurons responded to menthol, whereas Group 2 neurons did not. Group 3-5 are bradykinin responsive neurons that were insensitive to capsaicin. Neuronal profiles shown in Group 3-5 were found only in injured DRG neurons (ipsilateral CCI and ipsilateral SNL L5L6 cultures) and were absent in uninjured DRG (controls).
X-axis (Time in minutes): sequential application of pharmacological ligands monitored over an hour. Arrows indicate 15 s application of the following: KCl: 30mM potassium chloride, ACh: 1mM acetylcholine, ATP: 20uM ATP, BR: 10uM bradykinin, ME: 400uM Menthol, AITC: 100uM allyl isothiocyanate, C: 500nM capsaicin. Y-axis: Ratio of 340nM/380nM, is a measure of intracellular calcium levels.

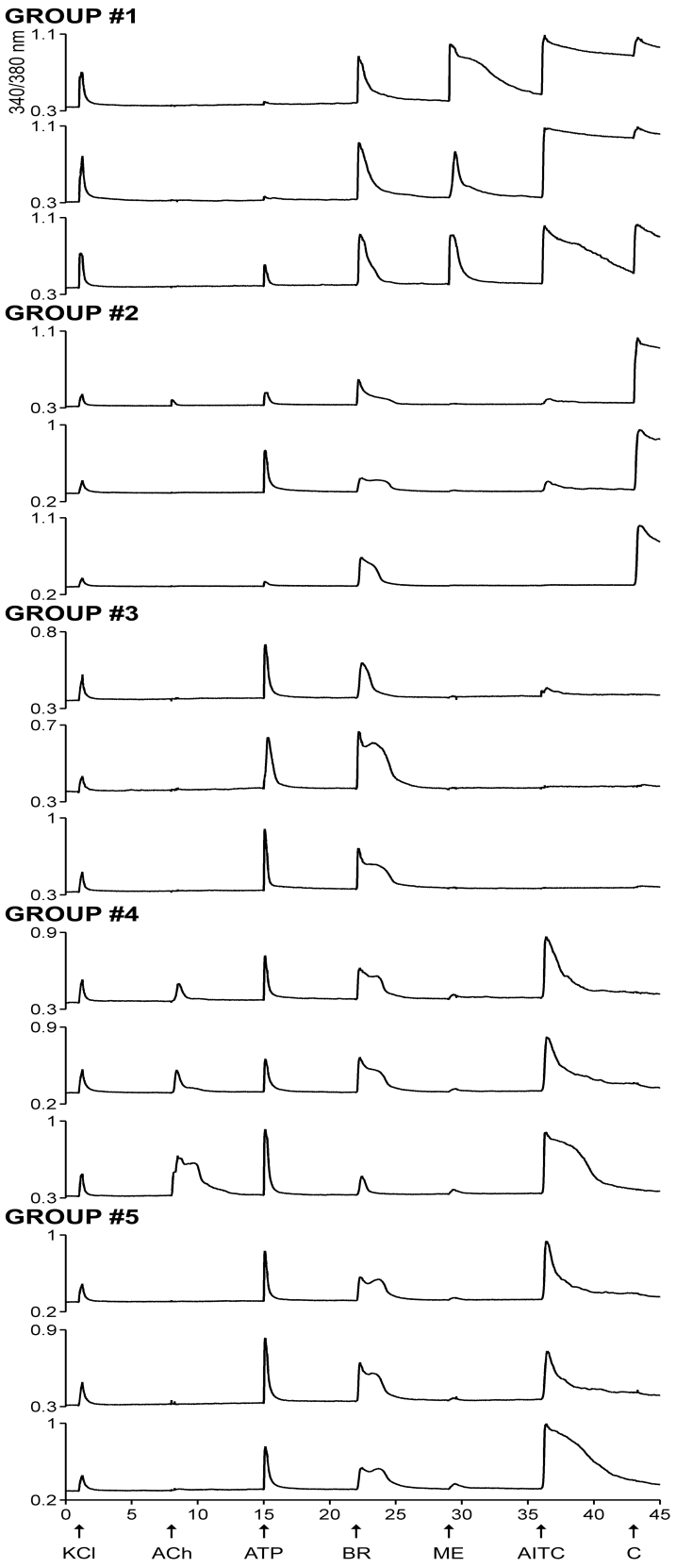
GROUP #1
340/380 nm
1.1
0.3
GROUP #2
1
0.2
GROUP #3
0.8
0.7
GROUP #4
0.9
GROUP #5
0
5
10
15
20
25
30
35
40
45
KCl
ACh
ATP
BR
ME
AITC
C

Figure 3.6: Quantitative analysis of bradykinin responsive neuronal phenotypes
A: Quantifying the appearance of new bradykinin responsive neurons in CCI and SNL DRGs. The phenotypic profiles of bradykinin responsive neuronal groups shown in Figure 3.5 were quantified. Groups 1 and 2 were found in all trials (injured experimental trials and uninjured control trials) and accounted for 12%±4% of the total neurons. In CCI and SNL injured DRG neurons, the net increase in bradykinin responsive neurons found 14 day post injury was accounted by the appearance of new phenotypes as shown in Figure 3.5 (Group#3-5). 30%±3% of the total neurons found in SNL ipsilateral L5L6 had phenotypic profiles of Group 3 and these phenotypic profiles appeared in injured CCI DRG with frequency of 11%±3% of the total neurons. Groups 4 and 5 also appeared only in injured SNL DRGs (4%±1% and 11%±2%, respectively) and CCI injured DRG (3%±1% and 5%±2%, respectively) and were absent in injured DRG. y-axis: Percentage of total neurons with phenotypic profiles shown in Figure 3.5, x-axis: Type of DRG tissue 14-days post-surgery. **B: Tracking the appearance of new bradykinin-responsive neuronal phenotypes in SNL DRGs with the progression of neuropathic pain:** The new bradykinin responsive neuronal groups (shown in Figure 3.5, Group # 3-5) did not appear on Day 1 and started to appear at Day 3, further upregulated at Day 6 and 14 after SNL injury. The progressive increase in bradykinin responsive neurons (as shown in Figure 3.4) is accounted by the appearance of new bradykinin responsive neuronal groups as shown here.

A

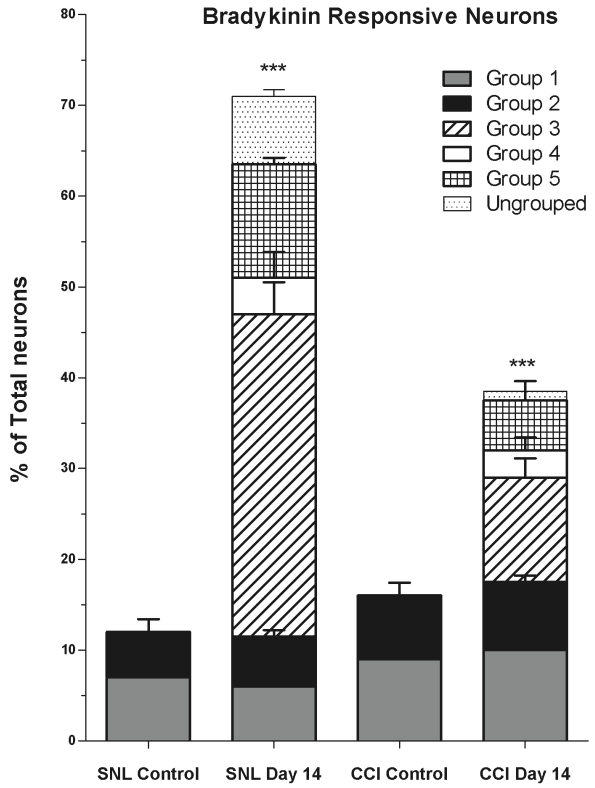
Bradykinin Responsive Neurons
% of Total neurons
80
70
60
50
40
30
20
10
0
***
***
Group 1
Group 2
Group 3
Group 4
Group 5
Ungrouped
SNL Control
SNL Day 14
CCI Control
CCI Day 14

B

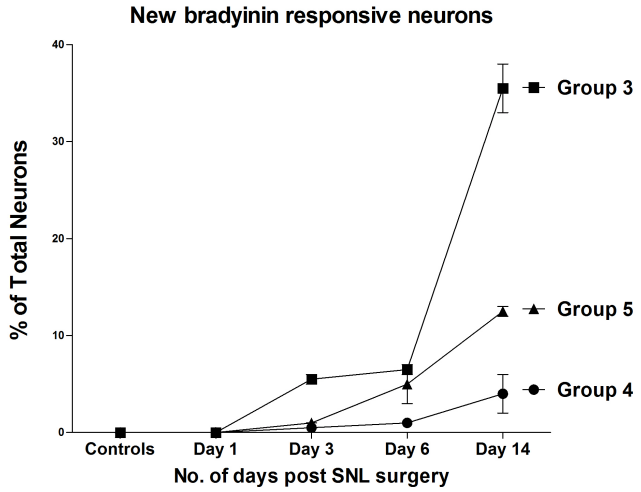
New bradyinin responsive neurons
% of Total Neurons
40
30
20
10
0
Group 3
Group 5
Group 4
Controls
Day 1
Day 3
Day 6
Day 14
No. of days post SNL surgery

Figure 3.7: Coordinated changes observed by comparing magnitude of responses
The neurons that responded to the application of both acetylcholine and ATP were compared. **A:** ACh and ATP responsive neurons in CCI cultures. A new bradykinin-responsive cell group appears in CCI cultures and a majority of these neurons had ATP response magnitude greater than ACh as shown in the last two traces. **C:** ACh and ATP responsive neurons in ipsilateral SNL L5L6. A majority of these neurons were bradykinin responsive and similar to neurons from CCI, the new cell group (Group #4 in Figure 2) appeared only in ipsilateral SNL L5L6 cultures and not in the controls. The percentage of neurons with ACh magnitude <ATP magnitude is significantly higher in ipsilateral SNL cultures. **B,D: Co-ordinated changes plotted on logarithmic scale to compare magnitudes of acetylcholine and ATP responsive neurons:**
The neurons represented in Figure 3.7A and 3.7C were plotted in logarithmic scale to compare the percentage of neurons based on the magnitude of responses to acetylcholine and ATP. X-axis is log scale of ACh:ATP. The vertical line represents the point where the magnitude of ACh and ATP are equal. The horizontal arrow determines the rank i.e. the percentage of neurons that have higher magnitude of ATP than ACh. Figure 3.7B: Comparison of ipsilateral CCI cultures with contralateral CCI. There is a leftward shift in ipsilateral CCI cultures indicating that more neurons have higher magnitude of ATP. The + symbols indicate that a lot of these neurons are bradykinin responsive (data from Figure 3.7A included) Figure 3.7D: Comparison of ipsilateral SNL L5L6 cultures with contralateral SNL L5L6 cultures. The plot reveals that not only a greater proportion of neurons (71% of ACh+ ATP+ neurons) have higher magnitude of ATP than ACh (leftward shift) compared to contralateral SNL L5L6 (7% of ACh+ ATP+ neurons) but also indicates a loss of neurons that have higher ACh magnitude than ATP in ipsilateral SNL L5L6 (29%) compared to contralateral SNL L5L6 (93%). These coordinated changes between ACh, ATP and BR suggest that appearance of new bradykinin responsive cell groups and loss of canonical ACh responsive groups could be causative of neuropathic pain. For Figure 3.7B, 614 neurons (163 BR responsive) from ipsilateral CCI were compared with 644 neurons (34 Br responsive) from contralateral CCI. For Figure 3.7D, 70 neurons (43 BR responsive) neurons from ipsilateral SNL L5L6 were compared with 173 neurons (5 BR responsive neurons) from contralateral SNL L5L6. The data were obtained from 14 CCI rats and 5 SNL rats, respectively.

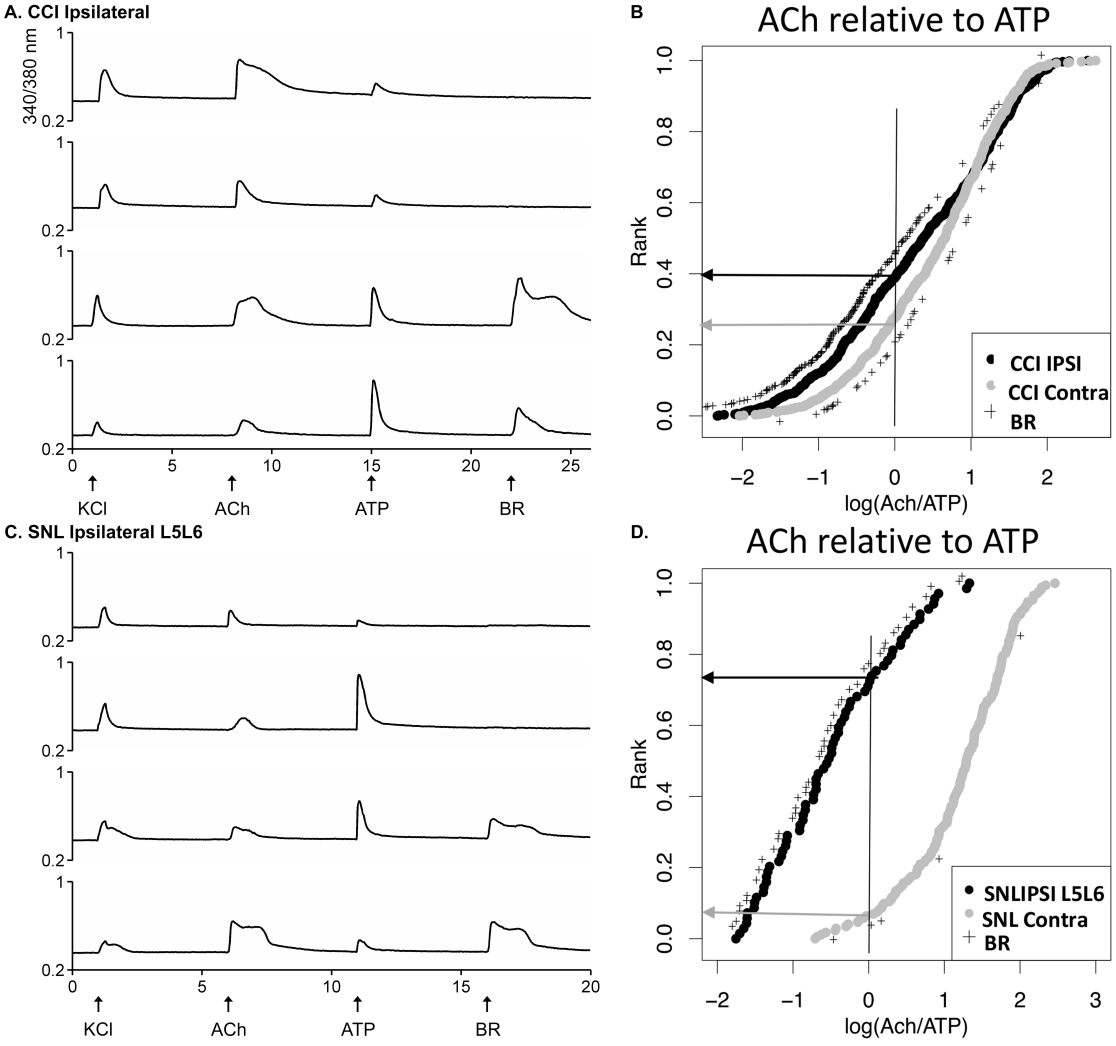
A. CCI Ipsilateral
340/380 nm
KCl
ACh
ATP
BR
B
ACh relative to ATP
Rank
log(Ach/ATP)
CCI IPSI
CCI Contra
BR
C. SNL Ipsilateral L5L6
KCl
ACh
ATP
BR
D.
ACh relative to ATP
Rank
log(Ach/ATP)
SNLIPSI L5L6
SNL Contra
BR

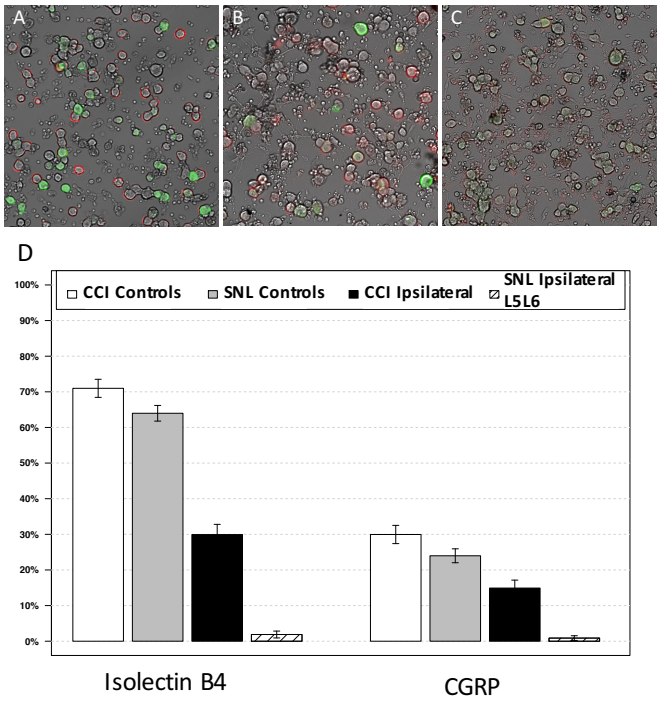

Figure 3.8: Effects of CCI and SNL injury on IB4 and CGRP stains
A, B, C are images of cell cultures obtained from control, ipsilateral CCI and ipsilateral SNL L5L6, respectively. The bright field image was overlaid with fluorescent images obtained for IB4 and CGRP staining. IB4 was conjugated to Alexa 546 dye (red) and the secondary antibody for anti-CGRP was conjugated with Alexa 488 dye (green). The percentage of neurons that were stained with IB4 and CGRP decreased with CCI and SNL injury as shown in **D**. For D, number of neurons compared are: ipsilateral CCI= 1019 neurons from 4 trials, control CCI=1282 neurons from 8 trials, ipsilateral SNL L5L6=797 neurons from 2 trials, control SNL=1910 neurons from 12 trials. Data obtained from 2 CCI rats, 2 SNL rats and 4 sham-operated rats.

Table 3.1: Summary of profiling experiments

The table describes the average percentage of neurons that responded to the application of other pharmacological agents in each tissue group. DRG neurons from injured ipsilateral CCI and ipsilateral SNL L5L6 are compared with the uninjured DRG from contralateral side and sham-operated rats. ACh= 1mM acetylcholine, ATP= 20uM ATP, BR= 10uM bradykinin, ME=400uM menthol, AITC= 100uM AITC, C= 500nM capsaicin. As shown in table, the percentage of acetylcholine and capsaicin responsive neurons significantly decreased in ipsilateral CCI and SNL L5L6 cultures and the percentage of ATP and bradykinin responsive neurons increased significantly. For CCI, data were obtained from 13 CCI-operated rats, 11 sham-operated rats and for SNL, data were obtained from 5 SNL and 4 sham-operated rats.

Summary of responses from DRG neurons 14-days post SNL injury							
		Average percentage of total neurons responsive to each stimulus (± S.E.M)					
Tissue group	**No. of Neurons**	**ACh**	**ATP**	**BR**	**ME**	**AITC**	**C**
Contralateral Sham L4	309	26% ± 4%	40% ± 6%	11% ± 4%	30% ± 6%	40% ± 6%	79% ± 4%
Contralateral Sham L5L6	277	29% ± 6%	64% ± 6%	13% ± 4%	28% ± 6%	36% ± 6%	77% ± 6%
Contralateral SNL L4	380	33% ± 4%	23% ± 4%	6% ± 2%	34% ± 4%	49% ± 6%	85% ± 4%
Contralateral SNL L5L6	960	33% ± 4%	44% ± 4%	12% ± 2%	25% ± 2%	33% ± 4%	74% ± 2%
Ipsilateral Sham L4	363	21% ± 4%	30% ± 4%	12% ± 4%	29% ± 4%	36% ± 6%	80% ± 4%
Ipsilateral Sham L5L6	714	27% ± 4%	55% ± 4%	12% ± 2%	29% ± 4%	38% ± 4%	73% ± 4%
Ipsilateral SNL L4	355	31% ± 4%	41% ± 6%	8% ± 2%	31% ± 4%	53% ± 6%	80% ± 4%
Ipsilateral SNL L5L6	1028	8% ± 2%	75% ± 2%	66% ± 2%	22% ± 2%	34% ± 2%	17% ± 2%
Summary of responses from DRG neurons 14-days post CCI							
		Average percentage of total neurons responsive to each stimulus (± S.E.M)					
Tissue group	**No. of Neurons**	**ACh**	**ATP**	**BR**	**ME**	**AITC**	**C**
Ipsilateral Sham	2002	25% ± 2%	45% ± 2%	20% ± 2%	28% ± 2%	39% ± 2%	63% ± 2%
Contralateral Sham	1805	23% ± 2%	42% ± 2%	20% ± 2%	32% ± 2%	39% ± 2%	65% ± 2%
Contralateral CCI	4982	30% ± 2%	47% ± 2%	17% ± 2%	31% ± 2%	42% ± 2%	66% ± 2%
Ipsilateral CCI	4713	21% ± 2%	64% ± 2%	34% ± 2%	32% ± 2%	47% ± 2%	49% ± 2%

References

1. Teichert RW, Schmidt EW, & Olivera BM (2015) Constellation pharmacology: a new paradigm for drug discovery. *Annual Review of Pharmacology and Toxicology* 55:573-589.

2. Ho Kim S & Mo Chung J (1997) Comparison of three rodent neuropathic pain model. *Experimental Brain Research.* 113(2):200-6.

3. Decosterd I & Woolf CJ (2000) Spared nerve injury: an animal model of persistent peripheral neuropathic pain. *Pain* 87(2):149-158.

4. Petho G & Reeh PW (2012) Sensory and signaling mechanisms of bradykinin, eicosanoids, platelet-activating factor, and nitric oxide in peripheral nociceptors. *Physiological Reviews* 92(4):1699-1775.

5. Curtice KJ*, et al.* (2016) Classifying neuronal subclasses of the cerebellum through constellation pharmacology. *Journal of Neurophysiology* 115(2):1031-1042.

6. Dube GR*, et al.* (2005) Loss of functional neuronal nicotinic receptors in dorsal root ganglion neurons in a rat model of neuropathic pain. *Neuroscience Letters* 376(1):29-34.

7. Levy D & Zochodne DW (2000) Increased mRNA expression of the B1 and B2 bradykinin receptors and antinociceptive effects of their antagonists in an animal model of neuropathic pain. *Pain* 86(3):265-271.

8. Reinhold AK*, et al.* (2015) Differential transcriptional profiling of damaged and intact adjacent dorsal root ganglia neurons in neuropathic pain. *PloS one* 10(4):e0123342.

9. Yarmolinsky DA*, et al.* (2016) Coding and Plasticity in the Mammalian Thermosensory System. *Neuron*.

10. Davis CL*, et al.* (1996) B1 bradykinin receptors and sensory neurones. *British Journal of Pharmacology* 118(6):1469-1476.

11. Bennett GJ & Xie YK (1988) A peripheral mononeuropathy in rat that produces disorders of pain sensation like those seen in man. *Pain* 33(1):87-107.

12. Kim SH & Chung JM (1992) An experimental model for peripheral neuropathy produced by segmental spinal nerve ligation in the rat. *Pain* 50(3):355-363.

13. Randall LO & Selitto JJ (1957) A method for measurement of analgesic activity on inflamed tissue. *Archives Internationales de Pharmacodynamie et de Therapie* 111(4):409-419.

14. King T*, et al.* (2009) Unmasking the tonic-aversive state in neuropathic pain. *Nature Neuroscience* 12(11):1364-1366.

15. Chaplan SR, Bach FW, Pogrel JW, Chung JM, & Yaksh TL (1994) Quantitative assessment of tactile allodynia in the rat paw. *Journal of Neuroscience Methods* 53(1):55-63.

16. Dixon WJ (1980) Efficient analysis of experimental observations. *Annual Review of Pharmacology and Toxicology* 20:441-462.

17. Qu C*, et al.* (2011) Lesion of the rostral anterior cingulate cortex eliminates the aversiveness of spontaneous neuropathic pain following partial or complete axotomy. *Pain* 152(7):1641-1648.

18. Burgess SE*, et al.* (2002) Time-dependent descending facilitation from the rostral ventromedial medulla maintains, but does not initiate, neuropathic pain. *Journal of Neuroscience* 22(12):5129-5136.

19. Xie JY*, et al.* (2005) Cholecystokinin in the rostral ventromedial medulla mediates opioid-induced hyperalgesia and antinociceptive tolerance. *Journal of Neuroscience* 25(2):409-416.

20. Navratilova E*, et al.* (2012) Pain relief produces negative reinforcement through activation of mesolimbic reward-valuation circuitry. *Proceedings of National Academy of Sciences USA* 109(50):20709-20713.

CHAPTER 4

A FAMILY OF EXCITATORY PEPTIDE TOXINS FROM VENOMOUS CRASSISPIRINE SNAILS: USING CONSTELLATION PHARMACOLOGY TO ASSESS BIOACTIVITY

Reprinted with permission from:

Julita Imperial, April Cabang, Jie Song, Shrinivasan Raghuraman, Joanna Gajewiak, Maren Watkins, Patrice Showers-Cornelli, Alexander Fedosov, Gisela P. Concepcion, Heinrich Terlau, Russell Teichert, Baldomero Olivera. Toxicon (2014). Vol 89. p45-54.

Published in final edited form as:
Toxicon. 2014 October ; 0: 45–54. doi:10.1016/j.toxicon.2014.06.014.

A Family of Excitatory Peptide Toxins from Venomous Crassispirine Snails: Using Constellation Pharmacology to Assess Bioactivity

Julita S. Imperial[a,*], **April B. Cabang**[b], **Jie Song**[c], **Shrinivasan Raghuraman**[a], **Joanna Gajewiak**[a], **Maren Watkins**[a], **Patrice Showers-Corneli**[a], **Alexander Fedosov**[d], **Gisela P. Concepcion**[b], **Heinrich Terlau**[c], **Russell W. Teichert**[a], and **Baldomero M. Olivera**[a]

[a]Department of Biology, University of Utah, 257 South 1400 East, Salt Lake City, UT 84112, USA

[b]Marine Science Institute, University of the Philippines, Diliman, Quezon City 1101, Philippines

[c]Institute of Physiology, University of Kiel, Hermann-Rodewald-Straße, 24118 Kiel, Germany

[d]A.N. Severtzov Institute of Ecology and Evolution, Russian Academy of Science, Moscow, 119071 Russia

Abstract

The toxinology of the crassispirine snails, a major group of venomous marine gastropods within the superfamily Conoidea, is largely unknown. Here we define the first venom peptide superfamily, the P-like crassipeptides, and show that the organization of their gene sequences is similar to conotoxin precursors. We provide evidence that one peptide family within the P-like crassipeptide superfamily includes potassium-channel (K-channel) blockers, the κP-crassipeptides. Three of these peptides were chemically synthesized (cce9a, cce9b and iqi9a). Using conventional electrophysiology, cce9b was shown to be an antagonist of both a human $K_V1.1$ channel isoform (Shaker subfamily of voltage-gated K channels) and a *Drosophila* K-channel isoform. We assessed the bioactivity of these peptides in native mammalian dorsal root ganglion neurons in culture. We demonstrate that two of these crassipeptides, cce9a and cce9b, elicited an excitatory phenotype in a subset of small-diameter capsaicin-sensitive mouse DRG neurons that were also affected by κJ-conotoxin pl14a, a blocker of $K_V1.6$ channels. Given the vast potential complexity of heteromeric K-channel isoforms, this study demonstrates that the crassispirine venoms are a potentially rich source for discovering novel peptides that can help to identify and characterize the diversity of K-channel subtypes expressed in native neurons and other cell types.

INTRODUCTION

One of the most biodiverse invertebrate lineages in the marine environment encompasses the venomous marine snails in the superfamily Conoidea, a group that by current estimates

*Corresponding Author: Julita S. Imperial; 257 S 1400 E, Salt Lake City, UT 84112; 801-581-8370; imperial@biology.utah.edu.

comprises more than 10,000 species (Bouchet et al., 2011; Olivera et al., 2014). Among these are the crassispirine neogastropods, a group long regarded as a subfamily of the family Turridae s.l. (McLean, 1971; Powell, 1966; Taylor et al., 1993), but in some more recent taxonomic work, included as a major clade within the family Pseudomelatomidae (Bouchet et al., 2011), an assemblage of venomous marine gastropods that encompasses more than 50 recent genera. These conoideans (which we will refer to as crassispirines or crassispirine snails) have generally been understudied and their toxinology is largely unknown. However, some crassispirine species were shown to possess hypodermic radular teeth, notably similar to those of cone snails (Kantor et al., 1997), suggesting a similar mechanism of prey envenomation.

In the Indo-Pacific, crassispirine snails are mostly collected offshore (in contrast to the Atlantic and Eastern Pacific, where a significant number of species live in shallow water). In recent years, access to live specimens of crassispirines from the Indo-Pacific has been provided by shell-gathering fishermen from the Philippines, who invented two novel methods for collecting snails from off-shore habitats. One such method is a gill net, a long fine-mesh net that is laid out overnight in deep water, typically at depths of 30-150m, and lifted before dawn. Many snails that happen to be on the nets as they are lifted become entangled within the net (for this reason, these are also called “tangle nets”) (Ng et al., 2009). A second method is to tie together old discarded fishing nets into a tight bundle, drop the bundle at the bottom and leave it for a period of two weeks to 6 months. These bundled nets, called *lumun-lumun* (Seronay et al., 2010), then become an ecosystem settled by small marine invertebrates. The richness of the net community that develops depends on the density of planktonic larvae that settle in the net, which is largely determined by the prevailing currents. When the nets are lifted, a large assortment of small molluscs (and other marine invertebrates) can be collected. Because of these innovations, routine access has been gained to live venomous crassispirine snails, making the first direct observations of their predatory behavior possible, as demonstrated in this study. In this paper, we describe the results of our studies on two species of crassispirine snails, *Crassispira cerithina* (Anton, 1839), a species that is routinely harvested from the *lumun-lumun* nets described above, and *Inquisitor intertincta* (Smith, 1877), which is generally collected using the gill net method.

The initial results of our toxinological investigation of these two species are presented here. The first family of venom peptides from the crassispirines, the κP-crassipeptides, has been defined by these studies. We also have utilized both conventional electrophysiology, as well as constellation pharmacology, a new approach for elucidating the biological activity of such families of venom peptides. In this study, we show that by simultaneously assaying a broad spectrum of receptors and ion channels expressed in a heterogeneous mixture of different cell types (Smith et al., 2013; Teichert et al., 2014a; Teichert et al., 2014b; Teichert et al., 2012a; Teichert et al., 2012b), we are able to assess bioactivity and provide an initial definition of the potential selectivity of newly-discovered venom peptides.

MATERIALS AND METHODS

Phylogenetic analysis of crassispirine snails

Using the SeaView package (Gouy et al., 2009), we aligned individual 12SrRNA, 16SrRNA, COI, sequences with Muscle (Edgar, 2004). We compared models of sequence evolution using PhyML (Guindon et al., 2010) and inferred maximum likelihood trees using the optimal GTR+I+G model (Tavaré, 1986) for the concatenated sequences of all three genes. Approximate Likelihood Ratio test (aLRT) statistics to provide branch length support for the trees (Guindon et al., 2010).

In addition, we used MrBayes (Huelsenbeck et al., 2001; Ronquist and Huelsenbeck, 2003) to infer model parameters and the tree using optimal partitioning for the concatenated sequences of all three genes. Each analysis comprised two simultaneous runs with four chains each for enough generations to reduce the average standard deviation of the split frequencies below 0.01 (about 17 million generations). Trees and parameters from the first 25% of the generations were discarded (the burn in) after completion of the MCMCMC (Metropolis Coupled Monte Carlo Markov Chain) search. Posterior Probabilities on the consensus tree provide branch support.

Identification and sequencing of cDNA clones encoding P-like crassipeptides

cDNAs were prepared by reverse transcription of RNAs from *Crassispira cerithina* and *Inquisitor intertincta*, venom ducts as previously described (Watkins et al., 2006). The resulting cDNAs were used as templates for polymerase chain reaction (PCR) using oligonucleotides corresponding to the conserved 5′ and 3′ UTR sequences of P-like prepropeptides. The resulting PCR products were purified using the High Pure PCR Product Purification Kit (Roche Diagnostics, Indianapolis, IN).

The eluted DNA fragments were annealed to pNEB206A vector using the USER Friendly Cloning kit (NewEngland BioLabs, Inc., Beverly, MA) following manufacturer's suggested protocol and the resulting products transformed into DH5α competent cells. The nucleic acid sequences of these P-like crassipeptide-encoding clones were determined according to the standard protocol for automated sequencing at the Health Sciences Center Core Sequencing Facility, University of Utah.

Chemical synthesis and oxidative folding of pl14a, cce9a, cce9b and iqi9a

The chemical synthesis of κJ-conotoxin pl14a was reported previously (Imperial et al., 2006), as was the chemical synthesis of cce9a (Cabang et al., 2011). The chemical synthesis of P-like crassipeptides cce9b and iqi9a was performed using methods described previously (Cabang et al., 2011). Briefly, both peptides were synthesized on an Apex 396 automated peptide synthesizer (AAPPTec, Louisville, KY, USA) using a standard solid-phase Fmoc (9-fluorenylmethyloxycarbonyl) protocol. The peptides were constructed on preloaded Fmoc-L-Val-Wang resin (substitution: 0.53 mmol g^{-1}, Peptides International Inc, KY, USA). The peptides were removed from the resin by treatment with reagent K (TFA/water/phenol/thioanisole/ethanedithiol 82.5/5/5/5/2.5 by volume) for 5 h (cce9b) and 4 h (iqi9a), subsequently filtered, precipitated and washed twice with cold methyl-tert-butyl ether. The

crude peptides were dissolved in 10% of solvent B and purified by RP-HPLC using a semi-preparative C_{18} Vydac column (218TP510, 250 mm × 10 mm, 5 m particle size) with a flow rate of 4 ml/min and a linear gradient ranging from 15% to 45% of solvent B in 30 min for cce9b and 20% to 50% of solvent B in 30 min for iqi9a. Solvents A and B were 0.1% (v/v) TFA in water and 0.1% TFA (v/v) in 90% aqueous acetonitrile, respectively. The absorbance of the eluate was monitored at 220/280 nm. The purity of peptides was assessed using an analytical C_{18} Vydac reversed-phase HPLC column (218TP54, 250 mm × 4.6 mm, 5 m particle size) with a flow rate of 1 ml/min and a linear gradient ranging from 15% to 45% of solvent B in 30 min for cce9b and 20% to 50% of solvent B in 30 min for iqi9a.

Oxidative folding of cce9b and iqi9a was performed as follows: the linear peptide was re-suspended in a 0.01% TFA solution and added to a solution containing: 0.1 M Tris-HCl (pH 7.5), 0.1 mM EDTA, 1 mM GSH and 1 mM GSSG. The final peptide concentration in the folding mixture was 20 M. The folding reaction was allowed to proceed for 64 min for cce9b and 24h for iqi9a, and then quenched by adding formic acid to a final concentration of 8%. The reaction mixture was separated by RP-HPLC on C_{18} columns with a linear gradient ranging from 15% to 45% and from 20% to 50% of solvent B in 30 min for cce9b and iqi9a respectively. The purity of the folded peptides was assessed using the method described for the linear peptides and was determined to be: 99% for cce9b and 96% for iqi9a. Both peptides were quantified by absorbance at 280 nm using an extinction coefficient (ε) value of 6990 $M^{-1}cm^{-1}$. Molecular mass was confirmed by ESI MS for cce9b: actual [MH+] = 3467.544, calculated [MH+] = 3467.487. Molecular mass was confirmed by MALDI MS for iqi9a: actual [MH+] = 3223.081, calculated [MH+] = 3223.299. The mass spectrometry data was collected at the Mass Spectrometry Core at the Salk Institute for Biological Studies in La Jolla, CA.

Constellation Pharmacology

The Constellation Pharmacology methods have been described in detail previously (Smith et al., 2013; Teichert et al., 2014a; Teichert et al., 2012a; Teichert et al., 2012b). Briefly, lumbar DRG neurons from a postnatal-day 22 mouse (C57BL/6) were removed, pooled and cells were dissociated by enzymatic and mechanical methods, after which the cells were cultured overnight. Cells were loaded with Fura-2-AM dye for calcium imaging. Responses were elicited from neurons by depolarizing the cells at regular time intervals with 25 mM extracellular potassium. Capsaicin (300 nM) was applied at the end of the experiment to identify neurons that express the TRPV1 channel (putative nociceptors). The crassipeptide cce9a (10 M) or the conopeptide pl14a (16 M) were applied to the cell culture while monitoring cytosolic calcium concentration by calcium imaging to determine whether these peptides directly elicited changes in cytosolic calcium concentration or altered the response to a depolarizing stimulus.

Assessment of *in vivo* effects

Each peptide sample was re-suspended in 12 l of saline solution. Using an insulin syringe the samples (5-10nmoles) were injected intracranially to mice that were 12-14 days old. The peptide-injected mice were observed side by side with saline-injected controls for at least 2 h. In these experiments, lethargy was assayed by pushing the mouse a few inches off its

resting position. The saline-injected mouse would go a few to several steps from where it lands; whereas, a lethargic mouse would stay put or move just a step or two from where it lands.

Electrophysiological recordings

The *Xenopus* expression system was used for investigating the potential effects of cce9a, cce9b and iqi9a on voltage-gated *Shaker* K^+ channels and human Kv1 channels (hKv1.1 - hKv1.7). Oocytes from *Xenopus laevis* were prepared as described previously (Jacobsen et al., 2000). Frogs were anaesthetized with 0.2% tricaine in ice water for surgery. cRNA coding for *Shaker*-K427D and hKv1 channels was injected and the oocytes were incubated 1-5 days to allow expression of the protein. Prior to the electrophysiological measurements, the vitelline membranes of the oocytes were removed mechanically with fine forceps. cRNAs encoding K^+ channels to be tested were prepared by standard methods as desribed in (Jacobsen et al., 2000). Whole cell currents were recorded under two-electrode voltage clamp control using a Turbo-Tec amplifier (npi electronic, Tamm Germany). The intracellular electrodes were filled with 2 M KCl and had a resistance between 0.5 and 1.2 MΩ. Current records were low-pass filtered at 1 kHz (-3dB) and sampled at 4 kHz. Leak and capacitive currents were corrected online by using a P/n method. The bath solution was normal frog Ringer's (NFR) containing (in mM): 115 NaCl, 2.5 KCl, 1.8 $CaCl_2$, 10 Hepes pH 7.2 (NaOH). Lyophilized peptides were dissolved in NFR, diluted to the final concentration and added to the bath chamber. All electrophysiological experiments were performed at room temperature (19-22 °C).

RESULTS

Biology and phylogenetics of crassispirine snails

There is little in the scientific literature that sheds light on the biology of the crassispirine snails; however, as shown in Figure 1, we have recorded observations of envenomation of worm prey by *Crassispira cerithina*, the crassispirine species that is the main focus of this study. The snail extends a pure-white proboscis when it approaches potential prey, and then injects a bolus of venom. Figure 1 was derived from a video taken by Dylan Taylor, which is the first record of envenomation by a crassispirine snail.

The initial member of the crassipeptide family defined in this study was initially discovered through the analysis of the venom ducts from *Crassispira cerithina* (Cabang et al., 2011). This was a peptide called cce9a. In this study, we report the discovery of cce9a homologs from both *Crassispira cerithina* and *Inquisitor intertincta*. These species belong to a monophyletic clade within the family Pseudomelatomidae that largely corresponds to the traditional subfamily Crassispirinae (Figure 2). The phylogenetic tree shows the relationships between these and other crassispirine species, using species from the closely related conoidean families, Drillidae and Clavatulidae, as outgroups. The tree is based on sequences from mitochondrial genes: 12SrRNA, 16SrRNA and COI. It strongly supports the close evolutionary relationship of *Crassispira cerithina* and *Inquisitor intertincta*.

Molecular cloning and synthesis of P-like crassipeptide sequences

Only one venom peptide has been reported from any species in the subfamily Crassispirinae, cce9a from *Crassispira cerithina* (Cabang et al., 2011). This 29 amino-acid peptide was purified from venom by following the bioactivity elicited when venom fractions and subfractions were injected into the mouse CNS. A partial sequence from a cDNA clone was previously obtained. Using this information, additional cDNA clones were analyzed from the venom ducts of *Crassispira cerithina* and *Inquisitor intertincta* as described in Materials and Methods. The results of the cDNA cloning revealed a set of peptides that are clear homologs, as shown in Table 1. The precursor sequences include a clearly defined signal sequence, an intervening propeptide sequence and a mature-peptide sequence at the C-terminus. The predicted mature-peptide sequences obtained from the cDNA clones are shown in Table 2. The amino-acid sequence of cce9a was also determined independently, using peptide purified from venom as previously reported (Cabang et al., 2011).

The sequences are consistent with what would be expected for members of the same venom-peptide superfamily in *Conus*; all of the peptides have a conserved arrangement of cysteine residues in their primary sequence (cysteine framework). This is very similar to the P-conotoxin family from *Conus* (Lirazan et al., 2000; Miles et al., 2002), where the cysteine framework of these peptides is designated as framework IX. We refer to this venom-peptide superfamily from crassispirines as the P-like crassipeptide superfamily. Three of the peptides shown in Table 2 (cce9a, cce9b and iqi9a) were chemically synthesized as described in Materials and Methods.

Evaluating the biological activity of P-like crassipeptides using Constellation Pharmacology

The synthetic crassipeptides (cce9a, cce9b and iqi9a) were tested for biological activity using the Constellation Pharmacology platform that was previously described (Teichert et al., 2014a; Teichert et al., 2014b; Teichert et al., 2012a; Teichert et al., 2012b). All three peptides caused excitatory effects in a subset of cultured lumbar dorsal root ganglion (DRG) neurons. Figure 3 demonstrates the effects of cce9a and cce9b in dissociated lumbar DRG neurons from a 22-day-old mouse. Notably, each calcium-imaging trace shown in Figure 3 represents the response of a different DRG neuron, from an experiment where the responses of more than 100 neurons were monitored simultaneously (selected traces are shown). The effects of cce9a were compared to another excitatory peptide, κJ-conotoxin pl14a (pl14a), from *Conus planorbis*, which is a blocker of the voltage-gated K channel, $K_V1.6$ (Imperial et al., 2006). The traces in Figure 3 demonstrate that cce9a specifically affected a subset of DRG neurons that were affected by pl14a. Although pl14a affected a relatively broader subset of DRG neurons, including large-diameter capsaicin-resistant neurons, the cce9a effects were limited predominantly to a subset of the small-diameter, capsaicin-sensitive DRG neurons (Figure 3) affected by pl14a.

In the experiments shown in figure 3, greater than 80% of the neurons in culture did not respond to either pl14a (the conopeptide) or to cce9a or cce9b (the crassipeptides). All of the cells that responded to the cce9a peptide (the lowest 6 traces) also responded to the pl14a peptide. However, there were a subset of cells (2nd to 4th traces from the top) which did not

respond to the cce9a peptide, but did respond to the pl14a peptide. Thus, the constellation pharmacology experiment shows that the cce9a peptide affected only a minority of DRG neurons, and all of the neurons affected were also affected by the pl14a peptide. However, the converse was not true; a subset of neurons were affected by pl14a, but not by cce9a. The effects elicited by cce9a and pl14a differed from one neuron to another, as illustrated in Figure 3, but included direct increases in cytosolic calcium concentration as well as amplification of responses to depolarizing stimuli. The conopeptide and the crassipeptide elicited the same types of effects in neurons that were affected by both. These effects are consistent with a variety of other K-channel blockers we have tested previously by the same method (Teichert et al., 2014a; Teichert et al., 2014b; Teichert et al., 2012a; Teichert et al., 2012b).

Using DRG neurons, the effects of cce9a, Iqi9a and cce9b were indistinguishable; the same subset of neurons were affected. When added sequentially, cce9a and cce9b elicited the same phenotypic response in the affected DRG neurons (see Figure 4 for specific examples).

In vivo effects; Electrophysiology of cce9b peptide

The results described above suggest that cce9a and cce9b may have identical molecular targets in mouse DRG cells, overlapping with the molecular targets of the pl14a *Conus* peptide. In order to evaluate the three peptides, cce9a, cce9b and iqi9a further, the synthetic peptides were injected into mice at doses between 5-10 nmoles. Both the cce9a peptide and the iqi9a peptide induced lethargy upon IC injection (see Methods). However, the cce9b peptide had strikingly different symptomatology. Increased excitability was observed — some of the mice exhibited barrel rolling or circling, while other mice had severely splayed legs. All of the mice were generally hypersensitive to touch. Thus, in the12-14 day old mice, very different behavioral symptomatology was observed with cce9a and cce9b, suggesting differences in targeting selectivity of these peptides. As shown in Table II, cce9b is more divergent in sequence from cce9a (iqi9a differs by two amino acid substitutions, while cce9b has 4 amino acid differences, all of which introduce positive charges). We therefore carried out an electrophysiological characterization of cce9a and cce9b in an effort to further define the divergence in molecular targeting specificity between the two peptides.

The calcium-imaging data strongly indicated that the crassipeptides might be K-channel blockers. We tested these peptides, by electrophysiology on the *Drosophila* Shaker and on human Kv1 channels (see Methods). This *Drosophila* channel has been used as a screen for K channel antagonists since it is generally more permissive in binding K channel antagonists compared to individual mammalian K channel subtypes. An inhibitory activity of the cce9b peptides on the *Drosophila* channel, with weaker activity on hKv1.1 was observed. Application of cce9b caused an inhibition of the current elicited by depolarization of the *Drosophila* Shaker-K427D and hKv1.1 channel (see Figure 5) with IC_{50} of 1.1 ± 0.2 μM and 2.9 ± 0.3 μM (mean ± S.E.M.; n=3) respectively. Other hKv1 channels tested (hKv1.2, hKv1.3, hKv1.4, hKv1.5, hKv1.6 and hKv1.7) were not affected by 1 μM cce9b (data not shown). These results establish that the cce9b peptide is a selective K-channel blocker. Both the cce9a and the iqi9a peptides (1 M) did not elicit any detectable effects when tested on these targets.

DISCUSSION

P-like crassipeptide superfamily

In this paper, we report the discovery of the first crassipeptide superfamily (P-like crassipeptides, Tables 1 and 2). We have demonstrated that multiple P-like crassipeptides can be expressed in the venom of a single crassispirine species (e.g. *Crassispira cerithina*) and that there are homologous P-like crassipeptides (Tables 1 and 2) found in different species of the former subfamily Crassispirinae (*Crassispira cerithina* and *Inquisitor intertincta*, Figure 2). The definition of the P-like crassipeptide superfamily demonstrates that the venom components in the crassispirine snails are generally similar to the venom peptides of *Conus*. The precursor organization is the same as in *Conus* peptides (Table 1) and the final gene product expressed in the venom is biochemically similar to P-conotoxins, which each have approximately 25 - 30 amino acids and three disulfide bonds (Table 2). The definition of the P-like crassipeptide superfamily and the functional characterization of a few of these peptides are the first steps toward the systematic exploration of this potentially rich pharmacological resource.

A few P-like crassipeptides were synthesized. The bioactivity of the synthetic peptides was first assessed using a platform that we have developed to facilitate discovery called Constellation Pharmacology. In the specific iteration used for these studies, the neuronal preparation used were dorsal root ganglion neurons in primary culture. The specific protocol applied, in which cells are loaded with Fura2 to assess changes in cytosolic calcium, and then pulsed with a KCl solution to induce membrane depolarization in all of the cells in the culture, leads to the simultaneous assessment of many different voltage-gated ion channels. Each dorsal root ganglion is believed to have ca. 25-30 different neuronal subclasses; the amount of calcium entry into the cytosol in a particular neuron will be a function of which isoforms of sodium channels, calcium channels and potassium channels expressed in that particular neuronal subclass. Thus, the protocols shown in Figure 3, allows 100-200 cells to be assayed simultaneously, with the activity of a peptide on all of the voltage-gated sodium, calcium and potassium channels simultaneously assessed. The advantage gained in using this assay is that because it is a high-content, phenotypic assay, if a particular venom peptide is selectively targeted to a specific channel isoform, only those neurons that express that channel isoform will be affected when the peptide is applied. The crassipeptides cce9a and cce9b exhibited similar effects in the same DRG neurons. It is not surprising that cce9a, from the venom of *Crassispira cerithina*, and iqi9a, from the venom of *Inquisitor intertincta*, exhibited similar effects, since these peptides only differ in two amino acids (Tables 1 and 2). Thus, two different species of crassispirine snails express in their venoms homologous P-like crassipeptides that presumably share the same native molecular targets in their prey (although there is no direct information available regarding the specific prey of *Inquisitor intertincta*).

We also found that cce9a and cce9b elicited effects that overlapped with the effects elicited by pl14a (Figure 3), a known blocker of a voltage-gated K channel, $K_V1.6$ (Imperial et al., 2006). It is notable that the two crassipeptides generally elicited the same specific cellular phenotypes as pl14a in the neurons affected. Since the pl14a peptide causes diverse

phenotypic responses in different DRG neuronal subclasses (see Figure 3), the correspondence in phenotypes suggests that in the neurons affected by pl14a and the crassipeptide, the molecular targets are identical. Notably, the majority of DRG neurons that did not respond to pl14a also were unresponsive to the crassipeptides. However, there was a subset of large DRG neurons that were affected by the pl14a conopeptide that were not affected by cce9a or cce9b (see Figure 3). These results suggest that pl14a has at least two molecular targets, only one of which is targeted by the crassipeptides. Additionally, cce9b blocked potassium currents mediated by the *Drosophila* Shaker K channel and the human $K_V1.1$ channel (Figure 4).

κP-crassipeptide family

Since the crassispirine snails are a large and diverse group, our results suggest that crassispirine venoms may become a rich source of K-channel-targeted ligands with novel targeting selectivity. As cce9a, cce9b and iqi9a appear to represent the first members of a novel crassipeptide family of K-channel inhibitors, we suggest adopting a nomenclature parallel to that for conopeptides. Thus, we name cce9a as κP-crassipeptide CceIXA, (where IX is the Roman numeral for "9"), with the peptide name abbreviated as κP_c-CceIXa. Since peptide names are often abbreviated, the family symbol for all crassipeptides for which a mechanism has been elucidated should be abbreviated with the subscript C, indicating that it is a crassipeptide. Similarly, the iqi9a and cce9b peptides will be designated κP-crassipeptide IqiIXA (κP_c-IqiIXA) and κP-crassipeptide CceIXB (κP_c-CceIXB), respectively.

Although we have defined the κP-crassipeptide family, it cannot be assumed that the uncharacterized members of the P-like crassipeptide superfamily (e.g. cce9c and iqi9b) are necessarily K-channel blockers. The sequences are significantly divergent (Table 2), raising the possibility that these peptides do not target K channels. The situation is analogous to that found in *Conus* venoms. One of the best-characterized groups of conotoxins is the O-superfamily, which includes ω-conotoxins that block Ca channels (Yoshikami et al., 1989), and κ-conotoxins that block K channels (Terlau et al., 1996). Similarly, some members of the P-like crassipeptide superfamily may not necessarily be K-channel blockers, and those that do not target K channels would not belong to the κP-crassipeptide family, although if cce9c and iqi9b target K channels, they would be assigned to the κP-crassipeptide family.

It is notable that although they are biochemically similar to conopeptides, the κP-crassipeptides are distinct from the diverse families of K-channel blockers characterized from *Conus* venoms so far. These include the κ-conotoxins (Terlau et al., 1996) that belong to the O-conopeptide superfamily, the κM-conotoxins (Chen et al., 2010) that belong to the M-conopeptide superfamily and the κJ-conotoxins (Imperial et al., 2006) that belong to the J-conopeptide superfamily. Although all of these have 2-3 disulfide bonds, they do not have the same cysteine pattern as the κP-crassipeptides. Thus, the putative K-channel blocking toxins from the crassispirine snails comprise a distinctive group of K-channel antagonists that diverge in structure and in their genetic origins from all of the diverse K-channel blocking peptides characterized from *Conus* venoms.

While cce9a, cce9b and iqi9a are analogous functionally to the various families of κ-conotoxins (κ-, κM- and κJ-conotoxin families), they have greater sequence similarity to the spasmodic peptides from molluscivorous cone snails that define the P-conotoxin superfamily (Lirazan et al., 2000; Miles et al., 2002). As shown in Table 2, there is a striking similarity in the spacing of cysteine residues in the two classes of peptides. This suggests that there may be structural similarity between these peptides, and that the P-like crassipeptides may fold into the ICK motif (inhibitory cysteine knot motif) that has been established for the P-conotoxin superfamily peptides (Miles et al., 2002).

This characterization of the P-like crassipeptides introduces a new paradigm for the discovery and characterization of novel pharmacologically active venom components. The discovery of bioactive compounds from the venoms of crassispirine snails presents special challenges compared to the traditional methods used for cone-snail venoms or milked-venom samples from other species. This is because many venomous crassispirine species are relatively small and often rare or difficult to collect. Therefore only a very limited amount of biological material is typically available. Although these limitations would have been impenetrable barriers to discovery just a few years ago, advances in molecular biology enable us to obtain venom-peptide sequences from even miniscule amounts of fresh tissue. Many of the crassispirine snails are between 5mm-2cm in length, but a single venom duct is now sufficient to obtain a rich harvest of venom-peptide sequences. Thus, the advances in molecular biology make it increasingly easy to obtain venom-peptide sequences. Furthermore, if the encoded venom peptides are under 40 amino acids in length, the chemical synthesis of the predicted peptides, while requiring specialized expertise, can be achieved successfully in most cases. Therefore, the on-going problems in venom-peptide discovery are generally not sequence discovery or peptide synthesis. Rather, the greater problems include how to prioritize which peptides are likely to have the most novel target selectivity and then to identify the targeting-selectivity profiles.

Target identification of bioactive venom peptides that elicit behavioral symptomatology can be particularly problematic. The elucidation of the mechanism that underlies the phenotype observed upon injection into animals can often take years. For example, it was previously known that cce9a was bioactive, since it caused a distinctive behavioral symptomatology: when injected into the central nervous system of adult mice, the peptide induced hyperactivity (Cabang et al., 2011). However, for cce9a, like many other venom peptides, the rate-limiting step has been the evaluation of the peptide's molecular targeting selectivity profile.

Constellation pharmacology

We are developing a form of high-content cell-based phenotypic screening assays that we refer to as "Constellation Pharmacology". The content of these high content assays is coupled to our on-going work to identify neuronal cell types and the cell-specific combinations of receptors and ion channels that they express (Smith et al., 2013; Teichert et al., 2014a; Teichert et al., 2014b; Teichert et al., 2012a; Teichert et al., 2012b). We refer to such cell-specific combinations of receptors and ion channels as "constellations" and

therefore the pharmacological approach to elucidate these cell-specific constellations as "constellation pharmacology".

We apply our knowledge of (and pharmacological markers for) cell-specific constellations to help identify the molecular targets of novel pharmacological agents, when we use native heterogeneous cell populations for high-content screening. Currently, we are using calcium-imaging for constellation pharmacology because we have successfully developed assays to interrogate a broad spectrum of receptors and ion channels by calcium imaging. However, we do not intend to use the term "constellation pharmacology" as a synonym for calcium imaging. Constellation pharmacology could potentially also be accomplished with high-throughput electrophysiology, imaging with voltage-sensitive dyes and other technologies. Through the on-going development of constellation pharmacology, we can assay a wide array of receptors and ion channels simultaneously across a heterogeneous cell population. As we apply more pharmacological markers to distinguish between cell types, we have a direct pathway for assessing whether a newly-discovered venom peptide differs in its molecular targeting specificity from already known pharmacological agents.

In this work, we used capsaicin as markers and the conopeptide pl14a, a $K_V1.6$ blocker to identify the neuronal subclasses affected by cce9a. We demonstrated that cce9a elicited an excitatory phenotype in a subset of the small-diameter capsaicin-sensitive DRG neurons that were also affected by pl14a (Figure 3). It is notable that the calcium-imaging approach used to assess bioactivity of cce9a also delimits its potential targeting selectivity compared to pl14a. Knowing which cells responded to cce9a, and which cells did not, provides a potential path to further identify the K-channel isoforms that are high-affinity targets for this peptide. The fact that pl14a affected a broader subset of DRG neurons suggests the possibility that cce9a may be more selective for certain heteromeric K-channel subtypes than pl14a, a hypothesis which will be tested in subsequent studies. As we progressively elucidate the cell-specific constellations of each cell type in a heterogenous cell population, such target discovery will be greatly facilitated.

It is also noteworthy that other cell populations, beyond DRG neurons, can be used for constellation pharmacology, which could also help to narrow the set of potential molecular targets (Raghuraman et al., 2014). Finally, we also note that although the purification of venom peptides was not reported in this work, the same approach can also be used for the bioassay-guided purification of venom components or other complex biological mixtures, as has been demonstrated in a companion study to this work (Aman et al., Manuscript in preparation).

Supplementary Material

Refer to Web version on PubMed Central for supplementary material.

Acknowledgments

This work was supported by a program project grant from the National Institute of General Medical Sciences (GM048677), by the Pharmaseas grant from the Republic of the Philippines (to GPC) and from the NIH/NIGMS Fogarty International Center's International Cooperative Biodiversity Groups (ICBG) grant (1U01TW008163). We

are grateful to Dylan Taylor for the videos of the behavior of *Crassispira cerithina*, from which the photographs shown in Figure 1 were derived.

REFERENCES

Anton, HE. Verzeichniss der Conchylien: welche sich in der Sammlung/von Hermann Eduard Anton befinden. Herausgegeben von dem Besitzer; Halle:Eduard Anton: 1839.

Bouchet P, Kantor Y, Sysoev AV, Puillandre N. A new operational classification of the Conoidea (Gastropoda). Journal of Molluscan Studies. 2011; (77):273–308.

Cabang AB, Imperial JS, Gajewiak J, Watkins M, Corneli PS, Olivera BM, Concepcion GP. Characterization of a venom peptide from a crassispirid gastropod. Toxicon. 2011; 58(8):672–80. [PubMed: 21939682]

Chen P, Dendorfer A, Finol-Urdaneta RK, Terlau H, Olivera BM. Biochemical characterization of kappaM-RIIIJ, a Kv1.2 channel blocker: evaluation of cardioprotective effects of kappaM-conotoxins. J Biol Chem. 2010; 285(20):14882–9. [PubMed: 20220134]

Edgar RC. MUSCLE: a multiple sequence alignment method with reduced time and space complexity. BMC Bioinformatics. 2004; (5):113. [PubMed: 15318951]

Gouy M, Guindon S, Gascuel O. SeaView version 4: A multiplatform graphical user interface for sequence alignment and phylogenetic tree building. Mol Biol Evol. 2009; 27(2):221–4. [PubMed: 19854763]

Guindon S, Dufayard JF, Lefort V, Anisimova M, Hordijk W, Gascuel O. New algorithms and methods to estimate maximum-likelihood phylogenies: assessing the performance of PhyML 3.0. Syst Biol. 2010; 59(3):307–21. [PubMed: 20525638]

Huelsenbeck JP, Ronquist F, Nielsen R, Bollback JP. Bayesian inference of phylogeny and its impact on evolutionary biology. Science. 2001; 294(5550):2310–4. [PubMed: 11743192]

Imperial JS, Bansal PS, Alewood PF, Daly NL, Craik DJ, Sporning A, Terlau H, Lopez-Vera E, Bandyopadhyay PK, Olivera BM. A novel conotoxin inhibitor of Kv1.6 channel and nAChR subtypes defines a new superfamily of conotoxins. Biochemistry. 2006; 45(27):8331–40. [PubMed: 16819832]

Jacobsen RB, Koch ED, Lang-Malecki B, Stocker M, Verhey J, van Wagoner RM, Vyazovkina A, Olivera BM, Terlau H. Single amino acid substitutions in κ-conotoxin PVIIA disrupt interaction with the *Shaker* K^+ channel. J. Biol. Chem. 2000; 275:24639–24644. [PubMed: 10818087]

Kantor YI, Medinskaya AI, Taylor JD. Foregut anatomy and relationships of the Crassispirinae (Gastropoda, Conoidea). Bull. Nat. Hist. Mus. (Zool.). 1997; 63:55–92.

Lirazan MB, Hooper D, Corpuz GP, Ramilo CA, Bandyopadhyay P, Cruz LJ, Olivera BM. The spasmodic peptide defines a new conotoxin superfamily. Biochemistry. 2000; 39:1583–1588. [PubMed: 10677206]

McLean JH. A revised classification of the family Turridae with the proposal of new subfamilies, genera and subgenera from the eastern Pacific. The Veliger. 1971; 14(1):114–130.

Miles LA, Dy CY, Nielsen J, Barnham KJ, Hinds MG, Olivera BM, Bulaj G, Norton RS. Structure of a novel P-superfamily spasmodic conotoxin reveals an inhibitory cystine knot motif. J. Biol. Chem. 2002; 277:43033–43040. [PubMed: 12193600]

Ng P, Mendoza J, Manuel-Santos M. Tangle net fishing, an indigenous method used in Balicasag Island, Central Philippines. The Raffles Bulletin of Zoology Supplement. 2009; 20:39–46.

Olivera BM, Showers Corneli P, Watkins M, Fedosov A. Biodiversity of Cone Snails and other Venomous Marine Gastropods: Evolutionary Success Through Neuropharmacology. Annual Review of Animal Biosciences. 2014; 2:487–513.

Powell AWB. The molluscan families Speightiidae and Turridae. Bulletin of the Auckland Institute and Museum. 1966; 5 1-184 + 23 plates.

Raghuraman S, Garcia AJ III, Anderson T, Twede V, Curtice KJ, Chase K, Ramirez J-M, Olivera BM, Teichert RW. Defining modulatory inputs into CNS neuronal subclasses through functional pharmacological profiling. Proc Natl Acad Sci U S A. 2014; 111(17):6449–6454. [PubMed: 24733934]

Ronquist F, Huelsenbeck JP. MrBayes 3: Bayesian phylogenetic inference under mixed models. Bioinformatics. 2003; 19(12):1572–4. [PubMed: 12912839]

Seronay RA, Fedosov AE, Astilla MA, Watkins M, Saguil N, Heralde FM 3rd, Tagaro S, Poppe GT, Alino PM, Oliverio M, Kantor YI, Concepcion GP, Olivera BM. Accessing novel conoidean venoms: Biodiverse lumun-lumun marine communities, an untapped biological and toxinological resource. Toxicon. 2010; 56(7):1257–66. [PubMed: 20005243]

Smith EA. Diagnoses of new species of Pleurotomidae in the British Museum. Annals and Magazine of Natural History. 1877; 4(19):488–501.

Smith NJ, Hone AJ, Memon T, Bossi S, Smith TE, McIntosh JM, Olivera BM, Teichert RW. Comparative functional expression of nAChR subtypes in rodent DRG neurons. Front Cell Neurosci. 2013; 7:225. [PubMed: 24348328]

Tavaré S. Some Probablsistic and Statistical Problems in the Analysis of DNA Sequences. American Mathematical Society: Lectures on Mathematics in the Lif Sciences. 1986; 17:57–86.

Taylor JD, Kantor Y, Sysoev AV. Foregut anatomy, feeding mechanisms, relationships and classifiction of the Conoidea (=Toxoglossa) (Gastropoda). *Bulletin, Natural History Museum, London* Zoology. 1993; 59(59):125–170.

Teichert RW, Memon T, Aman JW, Olivera BM. Using constellation pharmacology to define comprehensively a somatosensory neuronal subclass. Proc Natl Acad Sci U S A. 2014a; 111(6): 2319–24. [PubMed: 24469798]

Teichert, RW.; Olivera, BM.; McIntosh, JM.; Bulaj, G.; Horvath, MP. The Molecular Diversity of Conoidean Venom Peptides and their Targets: From Basic Research to Therapeutic Applications. In: King, GF., editor. Venom to Drugs: Venom as a Source for the Development of Human Therapeutics. RSC Publishing; London: 2014b.

Teichert RW, Raghuraman S, Memon T, Cox JL, Foulkes T, Rivier JE, Olivera BM. Characterization of two neuronal subclasses through constellation pharmacology. Proc Natl Acad Sci U S A. 2012a; 109(31):12758–63. [PubMed: 22778416]

Teichert RW, Smith NJ, Raghuraman S, Yoshikami D, Light AR, Olivera BM. Functional profiling of neurons through cellular neuropharmacology. Proc Natl Acad Sci U S A. 2012b; 109(5):1388–95. [PubMed: 22307590]

Terlau H, Shon K, Grilley M, Stocker M, Stühmer W, Olivera BM. Strategy for rapid immobilization of prey by a fish-hunting cone snail. Nature. 1996; 381:148–151. [PubMed: 12074021]

Watkins M, Hillyard DR, Olivera BM. Genes expressed in a turrid venom duct: divergence and similarity to conotoxins. Journal of Molecular Evolution. 2006; 62(3):247–56. [PubMed: 16477526]

Yoshikami D, Bagabaldo Z, Olivera BM. The inhibitory effects of omega-conotoxins on calcium channels and synapses. Ann. N.Y. Acad. Sci. 1989; 560:230–248. [PubMed: 2545135]

Highlights for crassipeptide paper

- Venom peptides from marine molluscs now extend from conotoxins to crassipeptides.
- This paper defines the first crassipeptide superfamily, the P-like crassipeptides.
- Three P-like crassipeptides were synthesized and characterized.
- The bioactivity of the characterized peptides suggests they are K channel blockers.

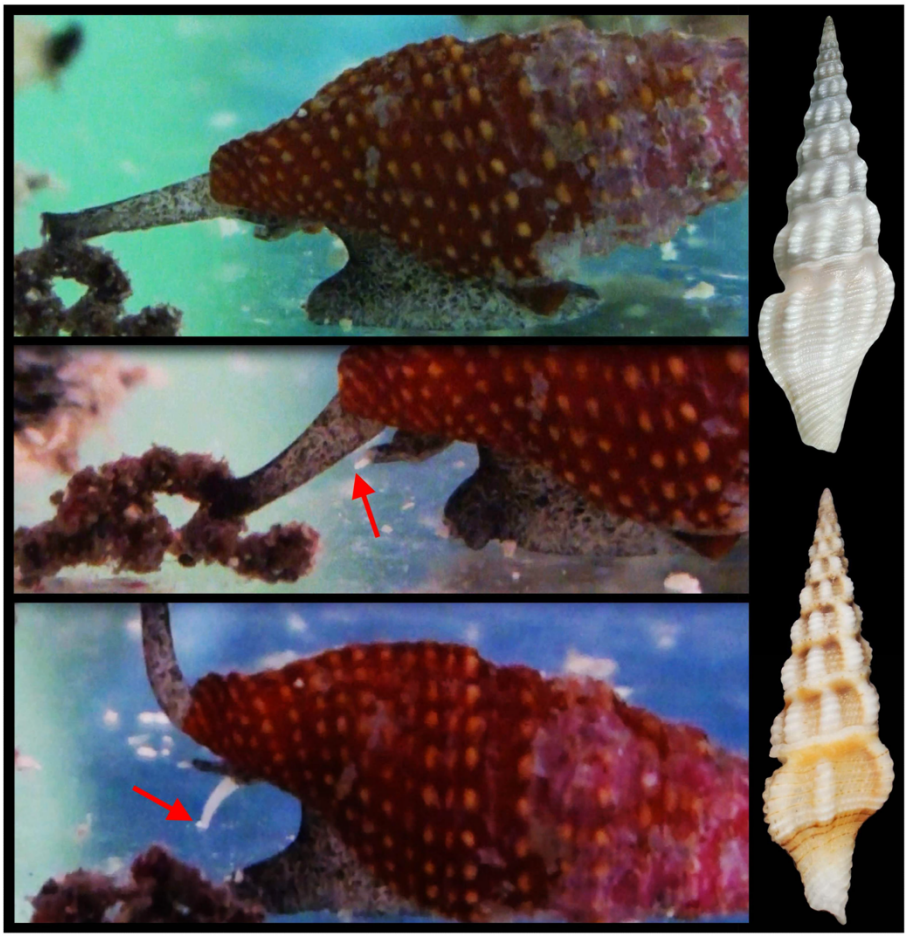

Figure 1.

eft panels: *Crassispira cerithina* attacking a worm. Top, the snail has its siphon extended; the snails use a chemosensory mechanism to locate their prey. Middle, the mouth parts of the snail are visible under the siphon, with the white tip of the proboscis (red arrows) extended out. Bottom panel: The extended white proboscis is clearly visible as the snail is ready to strike and inject its venom; the eye stalks of snails are also visible. Right panel. Representatives of the two other genera that group together with *Crassispira cerithina* in a monophyletic clade. Top, *Ptychobela lavina*; bottom, *Inquisitor intertincta*.

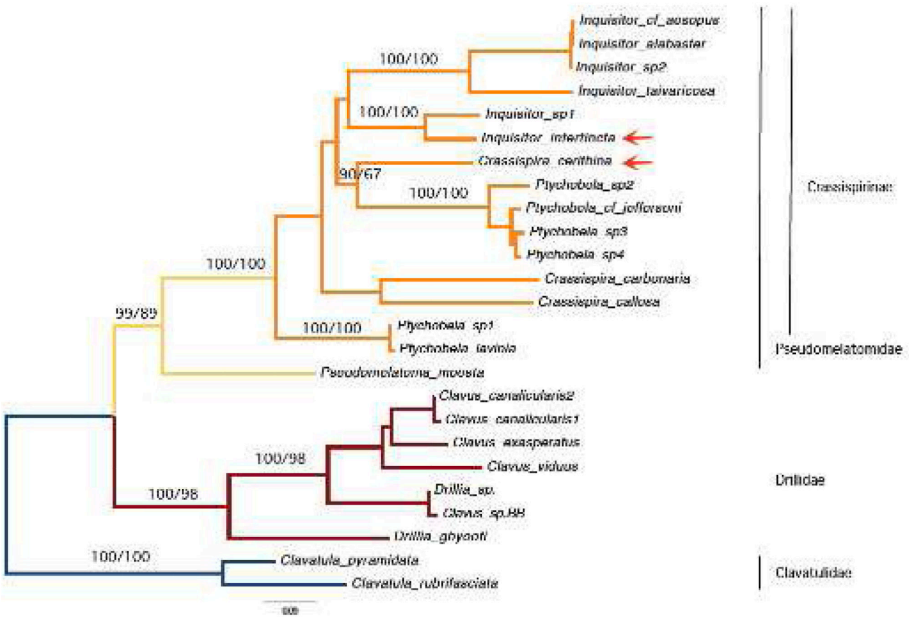

Figure 2.

The maximum likelihood tree showing the relationships of *Crassispira cerithina* and *Inquisitor intertincta* (red arrows) to other species in the Crassispirinae, a subfamily of the family Pseudomelatomidae (Bouchet et al., 2011) and to species in two other Conoidean families, Clavatulidae and Drillidae. Branches are labeled with Bayesian posterior probabilities (left) and approximate Likelihood Ratio (aLRT) statistics (right). The taxonomic assignments of species in the tree (*Crassispira*, *Ptychobela* and *Inquisitor*) are not consistent with the molecular phylogeny, and may need revision in the future once molecular data are obtained from more species.

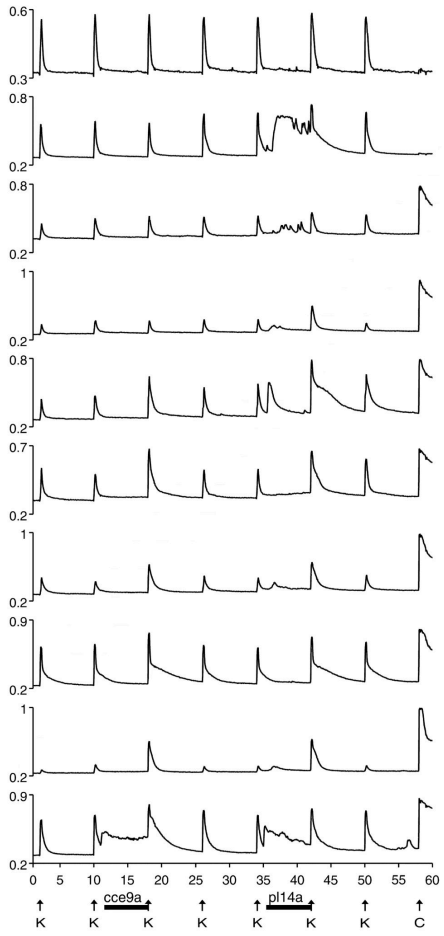

Figure 3.

The effects of cce9a and pl14a on a subset of DRG neurons. Selected calcium-imaging traces from dissociated DRG neurons show the diverse effects of a P-like crassipeptide, cce9a, and a conopeptide, κJ-conotoxin pl14a, a known blocker of a voltage-gated K channel, $K_V1.6$. Each arrow represents a 15-second application of either 25 mM extracellular potassium (K), to depolarize the neurons, or 300 nM capsaicin (C). Horizontal bars indicate when either cce9a (10 μM) or pl14a (16 μM) were present in the bath. (top trace) Responses from a large-diameter capsaicin-resistant neuron that was unaffected by

either cce9a or pl14a. (2nd trace from top) Responses from a large-diameter capsaicin-resistant neuron that was unaffected by cce9a. In contrast, pl14a elicited an increase in the baseline cytosolic calcium concentration that reversed after washout of the peptide. (3rd and 4th traces from top) Responses from two small-diameter capsaicin-sensitive neurons that were unaffected by cce9a. In contrast, pl14a elicited reversible increases in baseline cytosolic calcium concentration, and an amplification of the response to a depolarizing stimulus (K), in the case of the 4th trace. (bottom six traces) Responses from neurons that were affected by both cce9a and pl14a, typically with amplified responses to depolarization (K), but also in some cases with increases in baseline cytosolic calcium concentration (e.g. bottom trace). Notably, all of these neurons were small-diameter capsaicin-sensitive neurons. In a wide variety of DRG neurons, pl14a elicited or amplified responses, whereas cce9a only elicited or amplified responses in a subset of the small-diameter capsaicin-sensitive DRG neurons.

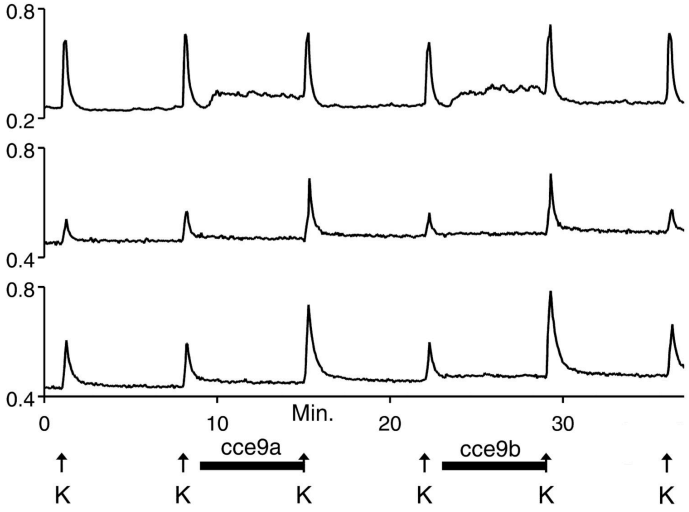

Figure 4.

The crassipeptides cce9a and cce9b amplified responses to a depolarizing stimulus or increased baseline Ca^{2+} concentration in largely the same DRG neurons (small-diameter neurons only). These effects were readily reversible. Arrows indicate brief applications of 20 mM K^{+} to depolarize the neurons. Each peptide was applied to the dissociated cell culture at 10 M concentration, as indicated by horizontal bars.

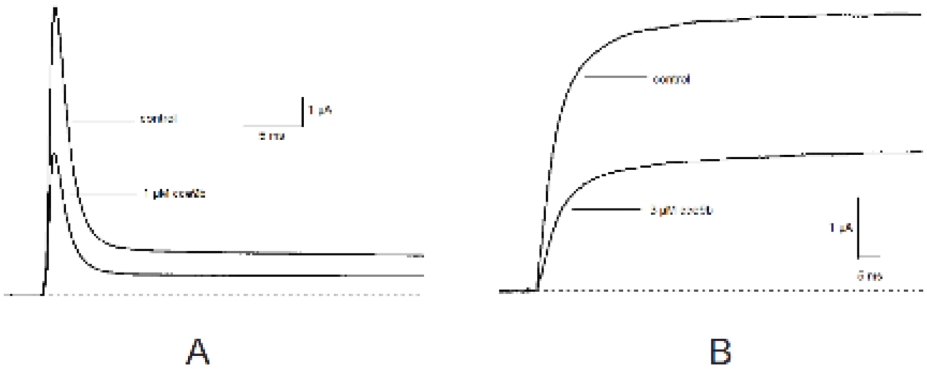

Figure 5.

The crassipeptide cce9b blocks *Shaker*- and hKv1.1-mediated currents. Whole cell currents recorded from an oocyte expressing *Shaker-K427D* (A) and an oocyte expressing hKv1.1 K^+ channels (B) evoked by test potentials to 10 mV. Addition of 1 μM of cce9b for *Shaker-K427D* and 3 μM for hKv1.1 results in a profound block of the currents. The dashed line corresponds to zero current. In contrast, addition of 1 μM of cce9a and Iqi9a had no effect (results not shown).

Table 1

Comparison of precursor sequences encoding P-like crassipeptides and P-conotoxins

Cloned P-like crassipeptide precursor sequences	
Cce9.1	MKLLPVLVTVVILLQLFADNHARVDGPRAVASGRYATKKAFLQMMTRGSCGLPCH-ENRRCGWACYCDDGICKPLRV*
IqI9.1	MKLLPVLVTVVILLQLFADNHARVDGPRAVASGRYATEKDFLQMMTRGSCGPPCH-ENRRCGWACYCDDGFCKPLRV*
IqI9.3	MKLLPVLVTVVILQQLFADNHARVAGPRPVASGQYATEKAFLQMIKRDVCSGSCY-YHYQCSRSCYCHYSHCRDKYEK*
Cce9 . 9	MKLLPVLVTVVILLQLFADNHARVDGPRAVANGRYATEKAFLQMMTRRFCGQSCHGQPSLCHWTCPCNGHFCSRL*
Cloned P-conotoxin precursor sequences	
tx9a	MHLSLARSAVLMLLLLFALGNFVVVQSGQITRDVDNGQLTDNRRNLQSKWKPVSLYMSRRGCNNSCQEHSDCESHCICTFRGCGAVNG*
gm9a	MHLSLARSAVLMLLLLFALGNFVVVQSGLITRDVDNGQLTDNRRNLQTEWNPLSLFMSRRSCNNSCQSHSDCASHCICTFRGCGAVNG*

The signal sequence is in blue. The propeptide sequence is in green. The mature-peptide sequence is in black. Stop codons are indicated by asterisks*.

Table 2

Comparison of mature-peptide sequences from P-like crassipeptides and P-conotoxins

Preliminary peptide name	Amino Acid Sequence	Peptide name following functional characterization
P-like crassipeptide sequences		
cce9a	GSCGLPCHEN-RRCGWACYCDDGICKPLRV	kP-crassipeptide CceIXA
iqi9a	GSCGPPCHEN-RRCGWACYCDDGFCKPLRV	kP-crassipeptide IqiIXA
cce9b	HSCRRHCHEN-RRCGWACYCDDGICKPLRV	kP-crassipeptide CceIXB
iqi9b	DVCSGSCYYH-YQCSRSCYCHYSHCRDKYEK	
cce9c	RFCGQSCHGQPSLCHWTCPCNGHFCSRL	
Alignment of P-conotoxin and P-like crassipeptide sequences		
tx9a (conotoxin)	GCNNSCQ□HSDC□SHCICTFRGCGAVN-NH_2	
gm9a (conotoxin)	SCNNSCQSHSDCASHCICTFRGCGAVN-NH_2	
cce9a	GACGLPCHENRRCGWACYCDDGICKPLRV	
iqi9b	DVCSGSCYYHYQCSRSCYCHYSHCRDKYEK	

Underlined amino acids indicate differences between cce9a, iqi9a and cce9b. Dashes are for alignment of amino acids. The cloned sequences shown in Table 1 encode some of the mature-peptide sequences shown here: Cce9.1 = cce9a, IqI9.1 = iqi9a, IqI9.3 = iqi9b, Cce9.9 = cce9c.

CHAPTER 5

CONCLUSION

Current drug discovery efforts focus on drug candidates acting on molecular targets identified from an established pathological state. The concerted molecular changes that occur in specific cell types during disease progression are generally undefined. Thus, systematically developing therapeutics for molecular targets whose function is required for disease progression is currently not feasible because neither the specific cell types, nor the critical molecular changes, have been identified. In this dissertation, I demonstrate the application of constellation pharmacology to address these problems.

In Chapter 2, the cell-specific constellations of major cell types were identified in neonatal mice VRC that form functional circuits to generate and maintain respiratory rhythm. The functional phenotypic diversity that was observed in dissociated cell culture was recapitulated in intact brainstem slice preparations and was validated by electrophysiological recordings from putative inspiratory neurons. This work highlighted the strength of constellation pharmacology in generating testable hypotheses and in obtaining novel modulators for physiologically relevant cell types (demonstrated for inspiratory neurons in this study). An extension of this work will focus on obtaining transgenic mice and labeling subsets of neurons (inspiratory, expiratory etc.) with genetically encoded fluorescent proteins to expand the information on constellation of ion channels and receptors expressed in shaping the phenotype of these cell types.

Chapter 3 demonstrates the use of constellation pharmacology platform to monitor changes to cellular phenotypes as a result of molecular changes that appear with the progression of pathological states. By using two models of neuropathic pain, CCI and SNL, I identified new groups of bradykinin responsive neurons that appeared in injured DRG. In addition, coordinated, multivalent molecular changes were observed that resulted in

phenotypic changes in different cell types. Opiates are the most commonly prescribed analgesics for neuropathic pain and there is an alarming increase in overdose-induced deaths and addiction. By elucidating the functional changes and properties of aberrant neuronal subtypes, we hope to devise suitable therapeutic interventions as an alternative to opiates.

The first (and key) step of identifying the appearance of aberrant neuronal phenotypes was achieved by using constellation pharmacology. As described before, ion channels and receptors exist in complex heteromeric isoforms that are largely neglected due to lack of selective pharmacological tools to study them. In Chapter 4, I demonstrate the applicability of constellation pharmacology to screen for novel pharmacological tools with potential for targeting ion channel subtypes. The activity of venom peptides (Cce9a and Cce9b) from a new family of venomous snails, *Crassispira cerithina*, was compared with previously characterized conotoxin (kJ-pl14a) from *Conus planorbis* by using constellation pharmacology and was found to target voltage-gated potassium channels.

Thus, in this dissertation, I establish the application of constellation pharmacology and 1) described different cellular phenotypes based on the membrane constellations, 2) investigated changes to cellular phenotypes in pathological conditions, and 3) discovered novel bioactive marine natural products that target complex isoforms of ion channels and receptors.